Study on superradiance in semiconductor high-quality thin films and nanoparticles

A dissertation submitted to

THE GRADUATE SCHOOL OF ENGIEERING SCIENCE

OSAKA UNIVERSITY

in partial fulfillment of the requirements for the degree of

DOCTOR OF PHILOSOPHY IN SCIENCE

BY

LE QUANG PHUONG

MARCH 2013

Acknowledgements

I am very grateful sincerely to my supervisor, *Prof. Masaaki Ashida*, for his continuous supports not only during this project but also for my proposed plans in future, for many useful advices and discussions, for providing me a freedom when I wanted as well as guidance when I needed it. Additional thanks for prompt and perfect corrections of our manuscripts.

My special thanks go to my advisors, *Dr. Masayoshi Ichimiya and Dr. Kensuke Miyajima*, for their uninterrupted supports, for guiding my first steps to establish the experimental measurements. Additional thanks for prompt and perfect corrections of our manuscripts.

I sincerely acknowledge *Prof. Hajime Ishihara* and *Prof. Tadashi Itoh* for their valuable help in every possible way through fruitful discussions and corrections of our manuscripts.

A special thanks to *Mr. N. Okamoto, Osaka Prefecture University* for preparing a programmed code to calculate linear response spectrum.

I would like to express my gratitude to members of Ashida Laboratory and Itoh Laboratory for their collaboration and friendship, which encouraged me to overcome many difficulties not only in my research but also in my life. I was lucky to have them for any required help and more...

Finally, without the continuous supports and endless love of my family, I would not have been the person I am. They were, are, and will be forever the most significant encouragement to me. Any words are not sufficient to express how important my beloved family means to me. This thesis is dedicated to them.

Abstract

This thesis focuses on exploring experimentally "superradiance" nature, in other words, exceptionally ultrafast optical responses, of excitons and biexcitons confined in semiconductor high-quality thin films and nanoparticles, respectively, by using various ultrafast optical spectroscopy methods.

In the first part of the thesis, CuCl thin films are grown by means of the molecular beam epitaxy method. Crystalline quality of the CuCl film including the surface morphology and the dephasing constant is extremely improved by our novel technique of electron beam irradiation at the beginning of MBE growth, and experiments using high-quality thin films with very small dephasing constants of about 0.2 meV can be feasibly realized. Then, by using the degenerate four-wave mixing and photoluminescence spectroscopy, superradiance of excitons confined in the high-quality CuCl thin films with thicknesses of a few hundred nanometers beyond the long-wavelength approximation is confirmed to be resulted from a remarkably long coupling length between light and multinode-type excitons which, in turn, could be controlled qualitatively just by changing the quality and thickness of CuCl thin films. Due to such kind of the coherent light-exciton coupling, photoluminescence signals

from the excitonic states corresponding to not only odd but also even quantum numbers, which are optically forbidden in the long-wavelength approximation, are clearly observed. The full width at half maximum of the excitonic state deduced qualitatively from the corresponding photoluminescence band shows almost the same dependence on the quantum number as the theoretical prediction about the ultrafast nature of light-coupled excitons. This result indicates that high coherence of matter systems is clearly reflected even in its incoherent photo-processes, which reveals unexploited potential of the PL spectroscopy and it also provides a clear example showing that the straightforward control of the size and quality of conventional materials can considerably enhance the degree of freedom enabling the development of novel material functions.

In the second part of the thesis, by generating a macroscopic coherent coupling between biexcitons confined in CuCl nanoparticles, superfluorescence emision, a particular case of superradiance, is observed successfully. As one of essential features for further understandings about biexciton superfluorescence emission from an ensemble of CuCl quantum dots observed recently, the radiative lifetime of biexcitons confined in 3-nm quantum dots is estimated to be about 80 ps under a two-photon resonant excitation by means of time-resolved Kerr gate spectroscopy. Different to the band-to-band excitation, the two-photon

resonant excitation is suggested to avoid efficiently the reabsorption process of biexciton luminescence from coexisting excitons leading to a possibility to observe successfully the pure lifetime of confined biexcitons. The obtained biexciton lifetime in nanoparticles is suggested to be suitable to support an occurrence of the superfluorescence emission.

TABLE OF CONTENTS

List of figures

List of abbreviations

AFM	Atomic force microscopy
c.m.	Center of mass
DFWM	Degenerate four-wave mixing
FWHM	Full width at half maximum
eV	Electron volt
kV	Kilovolt
LWA	Long-wavelength approximation
MBE	Molecular beam epitaxy
mm	Millimeter
nm	Nanometer
NPs	Nanoparticles
PL	Photoluminescence
QDs	Quantum dots
RHEED	Reflection High Energy Electron Diffraction
SF	Superfluorescence
SEM	Scanning electron microscope
TEM	Transmission electron microscope
μm	Micrometers

Chapter 1

Introduction

Nonlinear optics is given intensive attentions due to its promising applications in the area of laser technology, optical communication and data storage technology, etc. Attracted by advanced features caused by quantum confinement effect in nanostructures, numerous activities on nonlinear optical properties of nanoscaled materials, are proposed not only for understanding new fundamental science but also for potential hopes for applications in daily life such as optical devices, photonic circuits, and environmental sensor, medical diagnostics, etc. Among of them, various researches have been launched by the requirements for practical optical devices that can deal the deficiencies of conventional technologies. With a rapid development of nanoscience and nanotechnology, new optical devices, such as high-speed optical switch, high-speed modulator, etc. are expected to be possible for further advanced applications. However, to realize such kind of the optical devices, we have to face with the conventional trade-off problem between the response time and the nonlinear efficiency of materials. In a centrosymetric optical material, the response polarization

could be written as a sum of linear, third-order nonlinear, fifth-order nonlinear polarizations, etc. In this case, the nonlinearity of the material is determined primarily by the third-order nonlinear susceptibility $\chi^{(3)}$ because the fifth and higher order nonlinearities are conventionally much smaller than the third-order one.

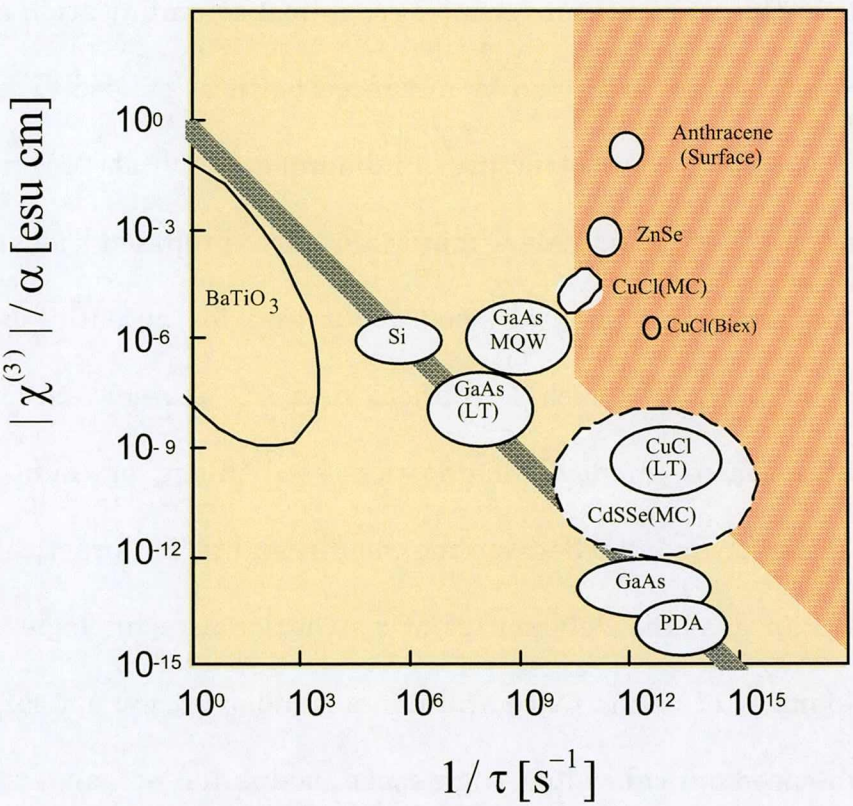

Figure 1.1. *The nonlinear efficiency which is determined by the fraction between the third-order nonlinear susceptibility $\chi^{(3)}$ and the absorption coefficient α as a function of the inverse of the response time τ. The shaded region corresponds to estimations made at low temperature.*

Figure 1.1 shows the third-order nonlinear efficiency determined by the fraction between the third-order susceptibility $\chi^{(3)}$ and the absorption coefficient α of some centrosymetric materials as a function of the inverse of the response time τ. The shaded region corresponds to estimations done at low temperature. It is obvious that for the materials whose have large nonlinear efficiencies such as $BaTiO_3$, Si, etc, the response times are slow. On the other hand, for the materials with small nonlinear efficiency such as CdSe, GaAs, PDA, the response times are much faster. Some materials such as CuCl, ZnSe show both high nonlinear efficiencies and fast response times but only at low temperature leading to infeasibility for practical applications.

As a consequence of the trade-off problem, to get a large nonlinear efficiency for real applications, materials with the slow response times should be chosen. However, in recently expected applications, for example, high-speed optical switch with a bit rate operation of about Tbit per second, the fast response time of the materials is essentially required. Let consider the following example to understand how important the fast response time is. Figure 2a shows the general principle of an optical switch. The on and off states of the optical switch is controlled optically by irradiating a strong gate pulse to the nonlinear optical material. With presence of the gate pulse,

the signal is allowed to pass through the nonlinear optical material. Otherwise, no signal is transmitted through the nonlinear optical material.

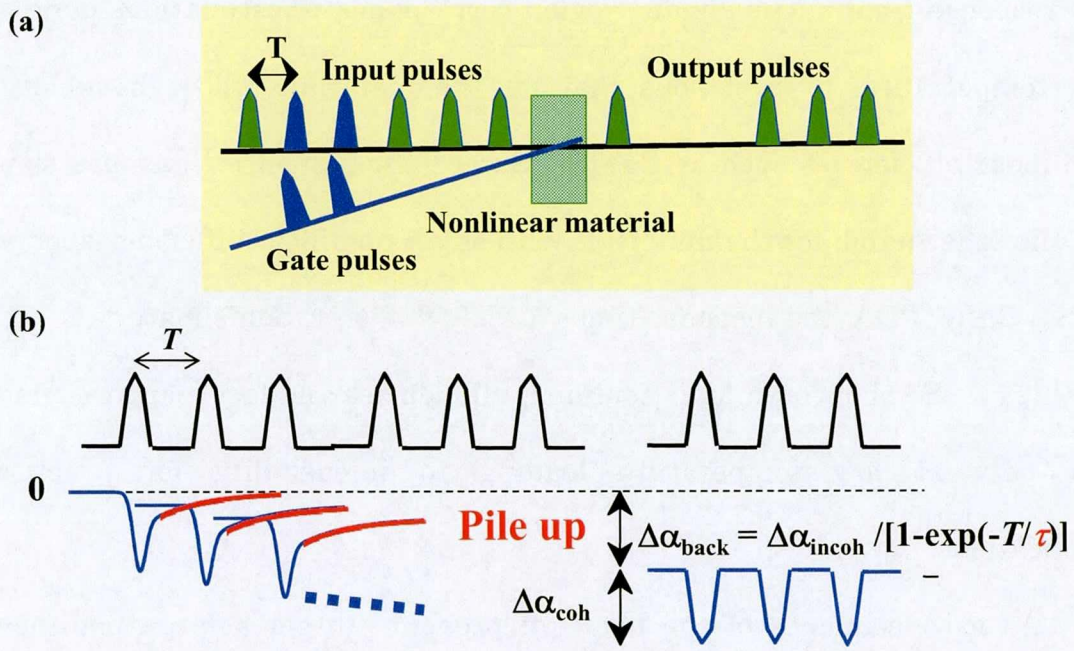

Figure 1.2. *(a) A schematic drawing of general principle of an optical switch. (b) Change in the absorption Δa caused by the incoherent different absorption Δa_{incoh} originated from the slow response time of the excited states in the materials when the nonlinear optical material operates at a high bit rate operation with the repetition time of T.*

However, if the operation rate of the nonlinear optical material determined by the repetition of the coming gate pulse is so high, for example in the order of Tbit per second, that the repetition time is comparable to or

smaller than the response time of the nonlinear optical material, the maximum operation rate of the nonlinear optical material then will be limited by the effect of the response time as discussed following. Figure 2b shows a schematic of the change in the absorption coefficient under a two-photon absorption process when the nonlinear optical material is irradiated by the gate light with a high bit rate. Besides the coherent different absorption $\Delta\alpha_{coh}$ caused by the two-photon process, there is the incoherent different absorption $\Delta\alpha_{incoh}$ caused by the slow lifetime τ of the excited state of excitations in the optical material. This incoherent different absorption tail then will be piled up with increasing the number of coming gate pulses and create a DC background of the different absorption $\Delta\alpha_{back}$ if the lifetime τ is comparable to the repetition time of the gate pulse. Because the modulation depth of the optical materials $\Delta\alpha_{coh}/\Delta\alpha_{back}$ have to be larger than 1, the maximum operation rate of the optical material will be determined as a function of the lifetime of excitations. As a result, the typical value of the maximum operation rate of semiconductor is about 10 Gbit per second, much slower than the expected one for recently advanced applications which is in the order of Tbit per second. Therefore, to realize high-speed control optical devices, fast response time is also essentially required. A lot of efforts, both theoretical and experimental, have done to find out efficient

ways to overcome the trade-off problem but still remain the fast response time.

In 1954, Dicke theoretically described a cooperative spontaneous emission from an ensemble of N two-level systems when the distance between any given pair of two-level systems is shorter than the emission wavelength as an optical phenomenon called superradiance [1]. Under a low excitation condition, if only one of the N two-level systems is excited, the transition rate of systems during superradiance is enhanced N times to that observed for an isolated two-level system [1]. The following theory has primarily been applied to study 'exciton superradiance' in condensed matter such as semiconductor quantum wells [2-3], quantum dots [4-5] and J-aggregates [6]: the transition rate of an exciton is enhanced by the accumulation of the dipole moments of the atoms present in the volume where coherence of center-of-mass (c.m.) motion of the exciton exists. These particular characteristics of superradiance give us possibility to obtain the ultrafast response time if the number of involved two-level systems N is large enough. Recently, besides experimental observation of exceptionally short radiative lifetime of light-coupled excitons in thin films [7], theoretical calculation predicts an extreme enhancement of the optical nonlinearity due to spatial interplay between light and multinode-type excitonic waves in semiconductor thin film [8]. As a result, superradiance phenomenon in

semiconductor nanostructures becomes very promising candidate for recently practical application of high-speed optical devices.

In this thesis, I focus on exploring experimentally "superradiance" nature, in other words, exceptionally ultrafast optical responses, of excitons and biexcitons confined in semiconductor high-quality thin films and nanoparticles, respectively, by using various ultrafast optical spectroscopy methods.

In the first part of the thesis, CuCl thin films are grown by means of the molecular beam epitaxy (MBE) method. Crystalline quality of the CuCl film including the surface morphology and the dephasing constant is extremely improved by our novel technique of electron beam irradiation at the beginning of MBE growth, and experiments using high-quality thin films with very small dephasing constants of about 0.2 meV can be feasibly realized. Then, by using the degenerate four-wave mixing (DFWM) and photoluminescence (PL) spectroscopy, superradiance of excitons confined in the high-quality CuCl thin films with thicknesses of a few hundred nanometers beyond the long-wavelength approximation is confirmed to be resulted from a remarkably long coupling length between light and multinode-type excitons which, in turn, could be controlled qualitatively just by changing the quality and thickness of CuCl thin films. Due to such kind of the coherent light-exciton coupling, photoluminescence signals from the

excitonic states corresponding to not only odd but also even quantum numbers, which are optically forbidden in the long-wavelength approximation, are clearly observed. The full width at half maximum of the excitonic state deduced qualitatively from the corresponding photoluminescence band shows almost the same dependence on the quantum number as the theoretical prediction about the ultrafast nature of light-coupled excitons. This result indicates that high coherence of matter systems is clearly reflected even in its incoherent photo-processes, which reveals unexploited potential of the PL spectroscopy and it also provides a clear example showing that the straightforward control of the size and quality of conventional materials can considerably enhance the degree of freedom enabling the development of novel material functions.

In the second part of the thesis, by generating a macroscopic coherent coupling between biexcitons confined in CuCl nanoparticles (NPs), superfluorescence (SF) emision, a particular case of superradiance, is observed successfully. As one of essential features for further understandings about biexciton superfluorescence emission from an ensemble of CuCl NPs observed recently, the radiative lifetime of biexcitons confined in 3-nm quantum dots is estimated to be about 80 ps under a two-photon resonant excitation by means of time-resolved Kerr gate spectroscopy. Different to the band-to-band excitation, the two-photon

resonant excitation is suggested to avoid efficiently the reabsorption process of biexciton luminescence from coexisting excitons leading to a possibility to observe successfully the pure lifetime of confined biexcitons. The obtained biexciton lifetime in NPs is suggested to be suitable to support an occurrence of the superfluorescence emission.

References

[1]. R. H. Dicke, Phys. Rev. **93**, 99 (1954).

[2]. J. Feldman, G. Peter, E. O. Gobel, P. Dawson, K. Moore, C. Foxcon and R. J. Elliot, Phys. Rev. Lett. **59**, 2337 (1987).

[3]. E. Hanamura, Phys. Rev. B **38**, 1228 (1988).

[4]. T. Itoh, M. Furumiya, T. Ikehara and C. Gourdon, Solid State Commun. **73**, 271 (1990).

[5]. M. Scheibner, T. Schmidt, L. Worschech, A. Forchel, G. Bacher, T. Passow and D. Hommel, Nat. Phys. **3**, 106 (2007).

[6]. H. Fidder, J. Knoester and D. A. Wiersma, Chem. Phy. Lett. **171**, 529 (1990).

[7]. M. Ichimiya, M. Ashida, H. Yasuda, H. Ishihara, and T. Itoh, Phys. Rev. Lett. **103**, 257401 (2009).

[8]. H. Ishihara and K. Cho, Phys. Rev. B **53**, 15823 (1996).

Chapter 2

Epitaxial growth of high quality CuCl thin films

CuCl thin films were grown by means of the molecular beam epitaxy (MBE) method. Crystalline quality of the CuCl films was extremely improved by our novel technique of electron beam irradiation at the beginning of MBE growth and experiments using high-quality thin films with small dephasing constants of about 0.2 meV and flat surface morphology can be feasibly realized. That is the high quality of thin films enables the excitonic wavefuncitons to extend coherently throughout the film volume leading to strongly harmonic couplings between the light and excitonic waves as discussed later in Chapter 3.

2.1. Introduction

Molecular beam epitaxy (MBE) is one of the most important methods not only for studying the surface film growth kinetics but also for fabrication of advanced electronic and optoelectronic devices. It is a versatile technique for growing thin epitaxial structures made of semiconductors, metals or insulators. The advantages of generally lower growth temperature and growth rate allow MBE to produce atomically abrupt heterojunctions and doping profiles leading to ability to fabricate many kinds of important devices such as high-speed microwave devices, metal based transistors, integrated circuit, and optoelectronic devices including lasers, LED, solar cell, etc [1].

CuCl is a well-known material for fundamental studies of exciton and biexciton properties at low temperature due to its simple band structure as well as large exciton, biexciton binding energies [2-3], but never thought to be suitable for any optically practical applications which usually operate at high temperature. However, recent theoretical calculation predicted an ultrafast radiative lifetime of excitons in CuCl thin films provided that the crystalline quality is sufficiently high so that the excitonic wavefunctions could extend coherently over the whole volume of the thin films [4-5]. This radiative lifetime was estimated to be much faster than the conventional

dephasing processes and supposed to recombine efficiently even at high temperature [6-7]. These results open a direct way to promote the CuCl, which has been utilized only for basic research, to promising material for application in the field of optical and electronic devices such as high-speed optical switch and modulator.

To realize the theoretical predictions, the first and most important step is to prepare high quality CuCl thin films. In this chapter, a method known as electron-beam-assisted MBE, which has been used to improve the epitaxial growth of GaAs, Si as well as Ge on CaF_2 substrate [8-13], is utilized to fabricate high quality CuCl thin film on CaF_2 substrate. As a result, high-quality thin films with very small dephasing constants (Γ) of about 0.2 meV can be feasibly realized for further experiments described in chapter 3.

2.2. Experimental details to chapter 2

2.2.1. Molecular beam epitaxial growth of high quality CuCl thin films

Figure 2.1 shows the general schematic diagram of the growth chamber of a MBE system. Its main elements are: sources of molecular beams; a manipulator

for heating, translating and rotating the sample; a cryoshroud surrounding the growth region; shutters to occlude the molecular beams; a gauge to measure chamber base pressure and molecular beam fluxes; a reflection electron diffraction (RHEED) gun and fluorescent screen to monitor film surface structure. The MBE growth process involves controlling, via shutters and source temperature, molecular and/or atomic beams directed at a single crystal sample suitably heated so as to achieve epitaxial growth. The gas background necessary to minimize unintentional contamination is predicated by the relatively slow film growth rate of approximately one micron per hour and is commonly in the 10^{-7}-10^{-8} Pa range. The mean free path of gases at this pressure and in the beam themselves is several orders of magnitude greater than the normal source-to-sample distance of about 20 cm. Hence, the beams impinge unreacted on the sample with a cryoshroud cooled by liquid nitrogen. Reactions take place predominantly at the sample surface where the source beams are incorporated into the growing film. Proper initial preparation of the sample will present a clean, single crystal surface upon which the growing film can deposit epitaxial. Timely actuation of the source shutters allow film growth to be controlled to the monolayer level. It is this ability to precisely control epitaxial film growth and composition that has attracted the intensive attention of material and device scientists.

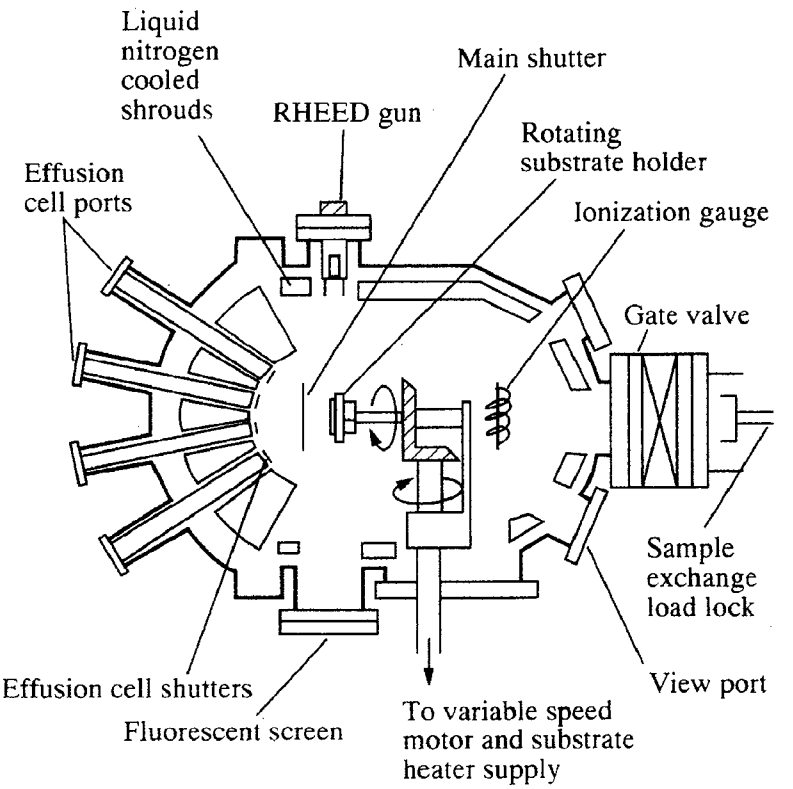

Figure 2.1. *A schematic diagram of a molecular beam epitaxy MBE system.*

Figure 2.2 shows a schematic diagram of the grown CuCl thin films. To grow CuCl thin film, a CaF_2 crystal was used as the substrate due to a very small difference between the lattice constants of CuCl (0.5406 nm) and CaF_2 (0.5463 nm). The 1mm-thick CaF_2 substrate cleaved along the (111) crystal plane then was attached to the substrate holder and placed inside the MBE growth chamber. After that, the CaF_2 substrate was heated up to 650 °C in 1 hour to remove chemical adsorptions from the CaF_2 substrate's

surface. The surrounding of the MBE growth chamber is cooled by a continuous flow of the liquid nitrogen to trap thermally the removed adsorptions or unwanted impurities and preserve the ultrahigh vacuum environment in the growth chamber throughout the fabrication process. After the thermal cleaning, a CaF_2 buffer layer with a thickness of about 40 nm was epitaxially grown at a growth rate of 0.4 nm/s upon the cleaned CaF_2 substrate kept at the temperature of 600 °C. The CaF_2 buffer layer and substrate then was cooled naturally down to the temperature of 130 °C.

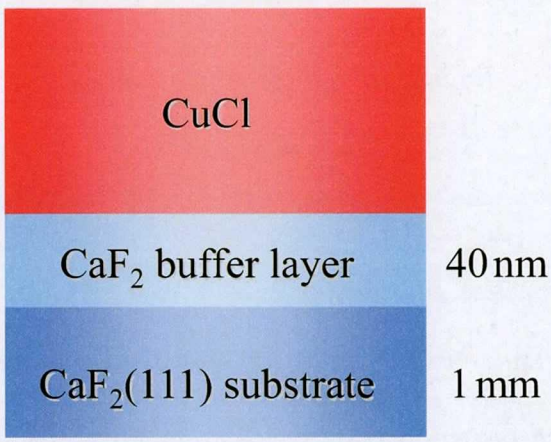

Figure 2.2. *A schematic diagram for the grown CuCl thin films including a CaF_2 substrate, a CaF_2 buffer layer and a CuCl layer.*

An electron beam emitted from the RHEED gun was accelerated by a high voltage of about 3-5 kV and then irradiated upon the CaF_2 buffer layer's surface in a few minutes. The electron beam was incident to the sample with a glancing angle of about 3° and it can be scanned on the sample along two directions. The electron beam exposure system is schematically shown in Fig. 2.3. After the electron beam irradiation, a CuCl layer with a thickness of a few hundred nanometers was grown epitaxially at a growth rate of 0.1 nm/s.

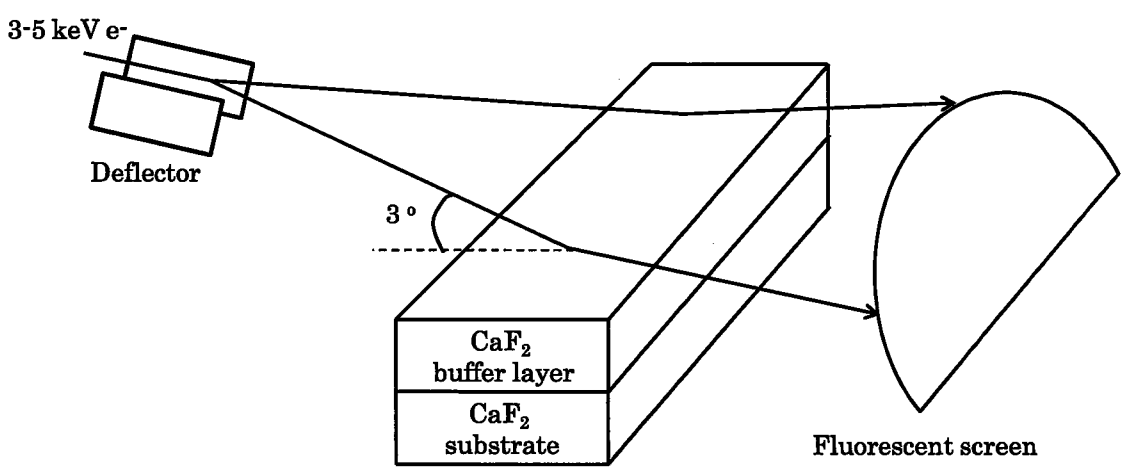

Figure 2.3. *Schematic drawing of an electron beam irradiation system. The electron beam can be scanned on the sample surface along two directions. Typical incident angle of the beam is 3°.*

2.2.2. Atomic force microscopy and reflection spectroscopy

To evaluate the crystalline quality of the grown CuCl thin films, it is impossible to use conventional tools such as transmission electron microscope (TEM) or scanning electron microscope (SEM) because the CuCl layer will be damaged easily under the irradiation of an electron beam accelerated by a voltage of several kV. Therefore, to examine the crystalline quality of the CuCl thin films, the atomic force microscopy (AFM) and reflection spectroscopy are suitable methods.

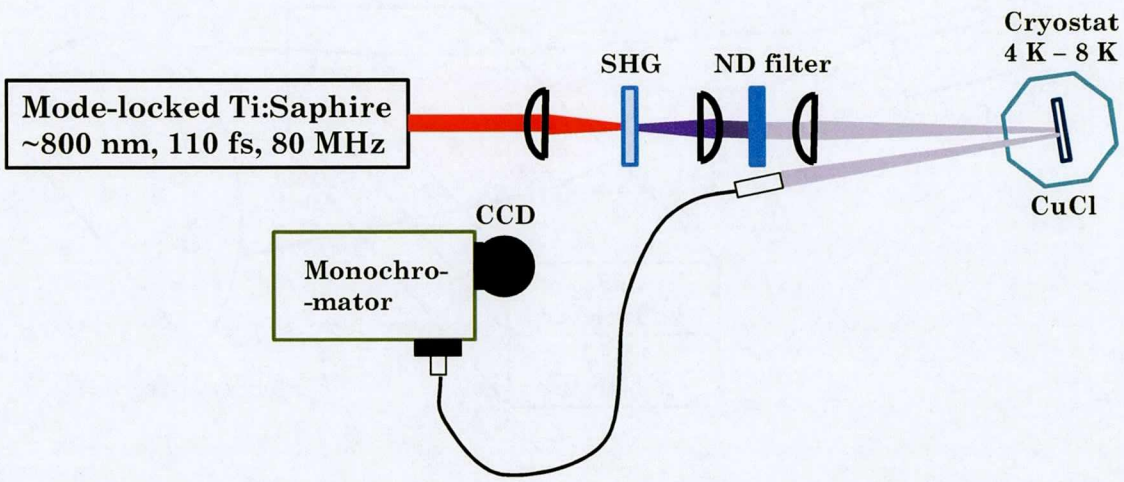

Figure 2.4. *A schematic diagram of the reflection measurement for CuCl thin films at low temperatures.*

The AFM image will give useful information about the surface morphology of the thin film. The surface morphology of the thin films was investigated in air by using an atomic force microscope, Seiko SPA 300 scanning probe unit controlled by SPI 3700 probe station. The AFM images then were usually obtained from a scanning area of 3 μm x 3 μm on the thin film surfaces by using the non-contact mode.

On the other hand, the film thickness and the dephasing constant at the measured spot were derived by fitting to the reflection spectra. The schematic diagram of the reflection measurement is shown in Fig. 2.4. In the reflection measurement, the second harmonic generation from a 110-fs mode-locked Ti: Sapphire was used as the incident beam. The photon energy was tuned to the excitonic resonant region of CuCl and the incident beam irradiated almost perpendicularly to the CuCl film's surface. The reflected beam then was directed to an optical fiber connected to a 50-cm monochromator equipped with a nitrogen-cooled CCD. It is should be noticed that the incident spot on the sample surface in the reflection measurement is exactly coincident with those in the degenerate four-wave mixing and photoluminescence measurement described later in Chapter 3.

2.3. High-quality CuCl thin films on CaF_2 substrate

2.3.1. Influence of electron beam irradiation on the film morphology

Figure 2.5b shows an image of a part of a grown CuCl thin film. The upper and the lower parts correspond to the grown CuCl thin film without and with an irradiation of electron beam, respectively. All other growth processes are the same for the upper and lower parts. Figure 2.5a and c present the corresponding AFM images of the upper and lower parts, respectively.

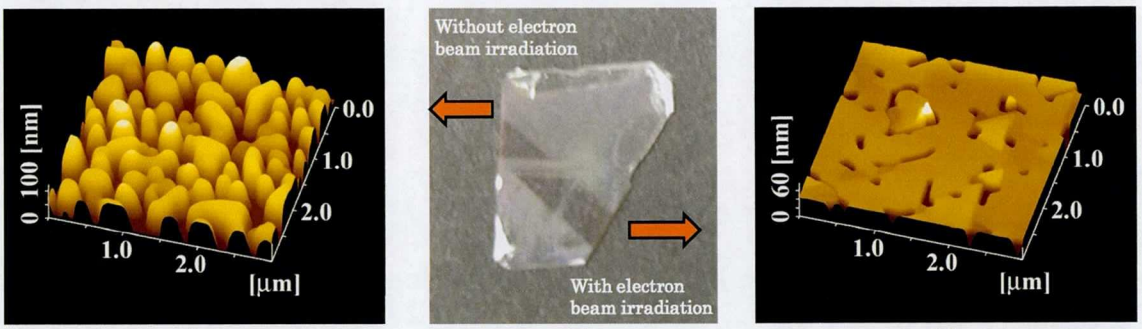

(a) (b) (c)

Figure 2.5. *(a) AFM image of the upper part of the thin film grown without an electron beam irradiation (b) Picture of the grown thin film where the upper and the lower parts correspond to the grown CuCl thin films without and with an electron beam irradiation. (c) AFM image of the lower part of the thin film grown with an electron beam irradiation.*

It is obvious that the thin film's surface condition with the electron beam irradiation on the CaF_2 buffer layer before the growth of CuCl layer is extremely improved than that without the electron beam exposure.

A great improvement of epitaxial growth of GaAs overlayers as well as Si, Ge overlayers on CaF_2 (111) after an electron-induced surface modification was already reported [8-13]. These results were well explained by assuming a desorption process of fluorine from the CaF_2 substrate leading to a generation of an ordered array of surface F centers on CaF_2 (111) which have a higher surface-free energy than the CaF_2 surface and should thus favor 2D growth of GaAs, Si and Ge on CaF_2. In a similar way for the case of CuCl growth on the electron irradiated CaF_2 buffer layer, the growth mechanism could be interpreted as following. The accelerated electrons remove the F^- ions locating near the CaF_2 buffer layer's surface, the empty positions left by the F^- ions then will be filled up by Cl^- ions during the growth of CuCl layer. This replacements result in a better wettability between the CaF_2 buffer layer and the subsequently grown CuCl layer then leading to a great improvement of the CuCl thin film morphology.

2.3.2. High-quality CuCl thin film on CaF_2 substrate

The AFM image of a 325-nm thin film's morphology irradiated with a 5-keV electron beam in 3 minutes is displayed in Fig. 2.6a. In addition, Fig. 2.6b shows the surface fluctuation along a crossed line on the surface of the corresponding film.

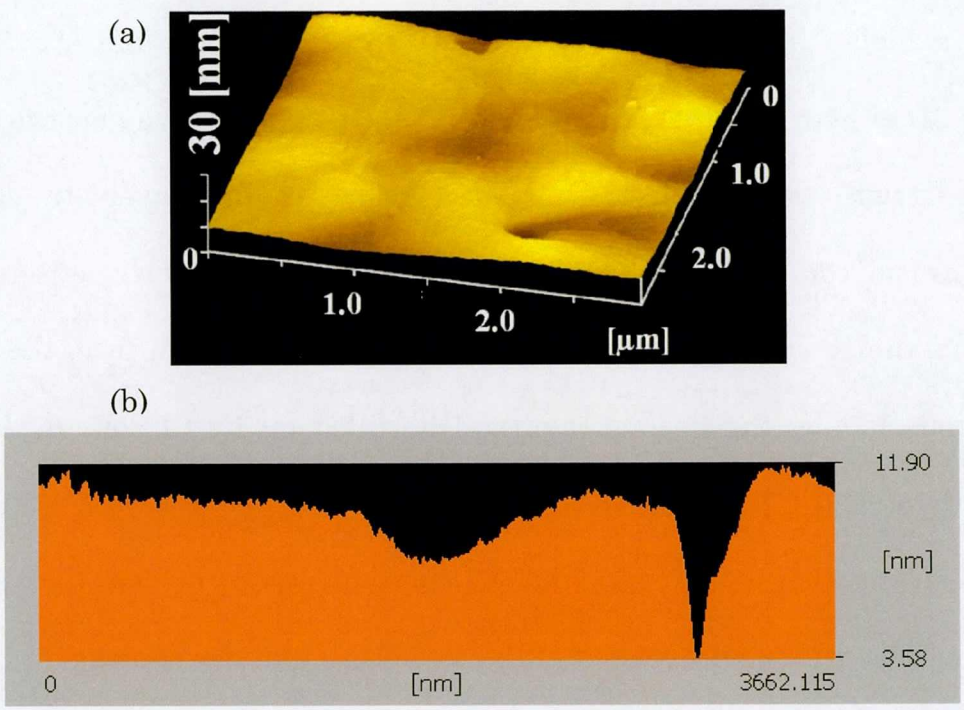

Figure 2.6. *(a) The atomic force microscopy image scanned over an area of 3 µm x 3 µm on a 325-nm thin film's surface with a vertical scale of 30 nm. (b) The fluctuation of the film surface along a crossed line on the surface.*

Roughness of the thin film at a flat region is estimated to be about 1-4 nm much smaller in comparison with the film thickness. Energy of the irradiated electron will determine the penetration depth of the electron inside the CaF_2 while the exposure time decides how many electrons are impinged onto the CaF_2 surface. Both of these parameters are supposed to affect primarily on crystalline quality of the CuCl overlayer. More details on the effects of these two parameters are in progress.

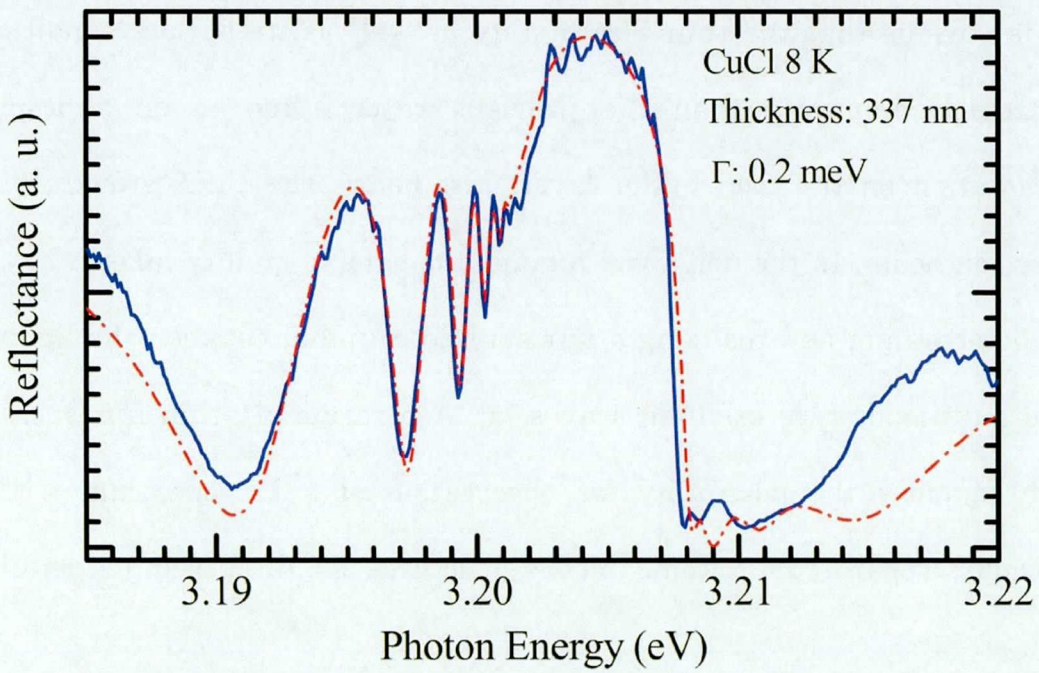

Figure 2.7. *A typical reflection spectrum of a CuCl thin fim (solid line) measured in the excitonic energy region at the same excitation spot as in the degenerate four-wave mixing and photoluminescence measurements. The dashed-dot line is the theoretically calculated fitting curve assumed for a dephasing constant Γ of 0.2 meV and a film thickness of 337 nm.*

A typical reflection spectrum of a high quality CuCl thin film measured with an incident light nearly perpendicular to the film surface is displayed in Fig. 2.7. The experimental data show a good agreement in the excitonic energy region with the theoretical calculation assumed for a small nonradiative dephasing constant Γ of 0.2 meV and a thickness of 337 nm. This value of the dephasing constant is quite smaller than that of samples used in the previous reports [14-16].

It is obvious that the thin film quality as well as its surface condition is extremely improved than the previous reports due to an appropriate irradiation on the CaF_2 buffer layer, just before the CuCl growth, of the electron beam. In the non-LWA regime, the sample quality takes a key role in determining and realizing a harmonized coupling between the light and the multimode-type excitonic waves [5]. A high quality thin film increases subsequently the possibility for observation of a PL spectrum with an obvious, separated excitonic mode structures as discussed in details in Chapter 3.

2.4. Summary

Crystalline quality of the CuCl films was extremely improved by our novel technique of electron beam irradiation on the CaF_2 substrate at the beginning of MBE growth of CuCl layer, and experiments using high-quality thin films with very small dephasing constants of about 0.2 meV can be feasibly realized. This electron-beam-assisted MBE method is expected to be useful to other type of materials with large excitonic effect, such as ZnO, GaN for exploring further feasible applications.

2.5. References

[1]. R. Farrow, *Molecular beam epitaxy: Application to key materials* (William Andrew, 1995).

[2]. K. Saito, M. Hasuno, T. Hatano, N. Nagasawa, "Band gap energy and binding energys of Z_3- excitons in CuCl", Solid State Commmun. **94**, 33 (1995).

[3]. H. Souma, T, Goto, T. Ohta, "Formation and radiative recombination of free excitonic molecule in CuCl by ruby laser excitation", J. Phys. Soc. Jpn. **29**, 697 (1970).

[4]. H. Ishihara, J. Kishimoto, K. Sugihara, J. Lumin. **108**, 343 (2004).

[5]. M. Ichimiya, M. Ashida, H. Yasuda, H. Ishihara, and T. Itoh, Phys. Rev. Lett. **103**, 257401 (2009).

[6]. M. Ichimiya, K. Mochizuki, M. Ashida, H. Yasuda, H. Ishihara, and T. Ioth, J. Lumin. **131**, 498 (2011).

[7]. M. Ichimiya, K. Mochizuki, M. Ashida, H. Yasuda, H. Ishihara, and T. Ioth, Phys. Status Solidi B **248**, 456 (2011).

[8]. S. Kanemaru, H. Ishiwara, and S. Furukawa, J. Appl. Phys. **63**, 1060 (1988).

[9]. A. Izumi, K. Tsutsui, and S. Furukawa, J. Appl. Phys. **75**, 2307 (1994).

[10]. P. O. Pettersson, R. J. Miles and T. C. McGill, J. Appl. Phys. **76**, 7328 (1994).

[11]. K. Kawasaki and K. Tsutsui, Appl. Surf. Sci. **117-118**, 753 (1997).

[12]. R. Benewitz, D. Smith and M. Reichling, Phys. Rev. B **59**, 8237 (1999).

[13]. B. R. Schroeder, S. Meng, A. Bostwick and M. A. Olmstead, Appl. Phys. Lett. **77**, 1289 (2000).

[14]. A. Syouji, B. P. Zhang, Y. Segawa, J. Kishimoto, H. Ishihara, K. Cho, Phys. Rev. Lett. **92**, 257401 (2004).

[15]. Z. K. Tang, A. Yanase, Y. Segawa, N. Matsuura, and K. Cho, Phys. Rev. B **52**, 2640 (1995).

[16]. M. Ichimiya, M. Ashida, H. Yasuda, H. Ishihara, and T. Itoh, Phys. Stat. Sol. B **243**, 3800 (2006).

Chapter 3

Superradiance of light-coupled excitons in high quality CuCl thin films

---

In this chapter, I report the observation of multiple light-coupling modes of excitons confined in CuCl thin films with thicknesses of a few hundred nanometers beyond the long-wavelength approximation in photoluminescence spectra. Due to a remarkably long coupling length between light and multinode-type excitons resulted from very high crystalline quality of thin films, photoluminescence signals from the excitonic states corresponding to not only odd but also even quantum numbers, which are optically forbidden in the long-wavelength approximation, are clearly observed. The full width at half maximum of the excitonic state deduced qualitatively from the corresponding photoluminescence band shows almost the same dependence on the quantum number as the theoretical prediction about the ultrafast nature of light-coupled excitons.

3.1. Introduction

3.1.1. Strongly harmonic coupling between light and multinode-type excitonic waves in high quality thin films

Quantum confinement effects of excitons in semiconductor systems with reduced dimensions have attracted considerable attention because of their potential applications to nonlinear optical devices, and as a means of exploring the basic physics of the quantized excitonic states [1]. In a strong confinement regime, where the exciton Bohr radius is larger than the size of the nanostructure, the electrons and holes are individually confined leading to quantization of their energy levels in different subbands. Excitons then are formed between quantized electron and hole levels. The excitonic transitions are optically allowed for the same quantum numbers ($n_e = n_h$) of the electron (n_e) and the hole (n_h) [2]. On the other hand, in a weak confinement, where the exciton Bohr radius is smaller than the size of the nanostructure, the picture of the confinement of the excitonic center of mass (c.m.) motions suitable for investigating the optical processes. In the framework of the long-wavelength approximation (LWA), wherein the spatial structure of the light wave is neglected by assuming a much longer light wavelength than the excitonic coherent length, excitonic transitions obey the parity selection rule that only the excitons with odd-parity wave

functions are optically allowed and the lowest state is most strongly coupled with light as shown in Fig. 3.1a [3]. Under this framework, the light-matter interaction is size-linearly enhanced and then saturated by the excitonic coherent length, because of the violation of c.m. confinement due to the dephasing, or by the wavelength of the resonant light, because of the phase mismatch between the lowest optically allowed exciton and the light wave [4-5].

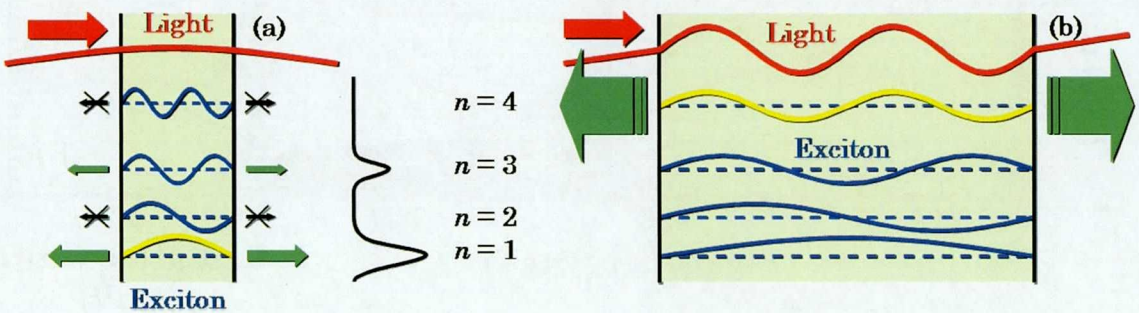

Figure 3.1. *(a) A schematic drawing of the multinode-type excitonic waves (yellow and blue solid lines) with different quantum numbers denoted nearby inside a semiconductor nanostructure belonging to the long-wavelength approximation where the light wavelength (red solid line) is much longer than the size of the nanostructure. Only odd-parity waves are optically allowed presented by green arrows. (b) A schematic drawing of the multinode-type excitonic waves extending coherently through a semiconductor nanostructure whose size is comparable to the light wavelength. Spatial interactions between the light and excitonic waves become important leading to the breakdown of the long-wavelength approximation.*

However, the coherent length of the exciton state can be very long in adequately high quality nanostructure. In this case, the spatial structures of the light can be no longer neglected leading to consequently the breakdown of the LWA, for example as shown in Fig. 3.1b [6].

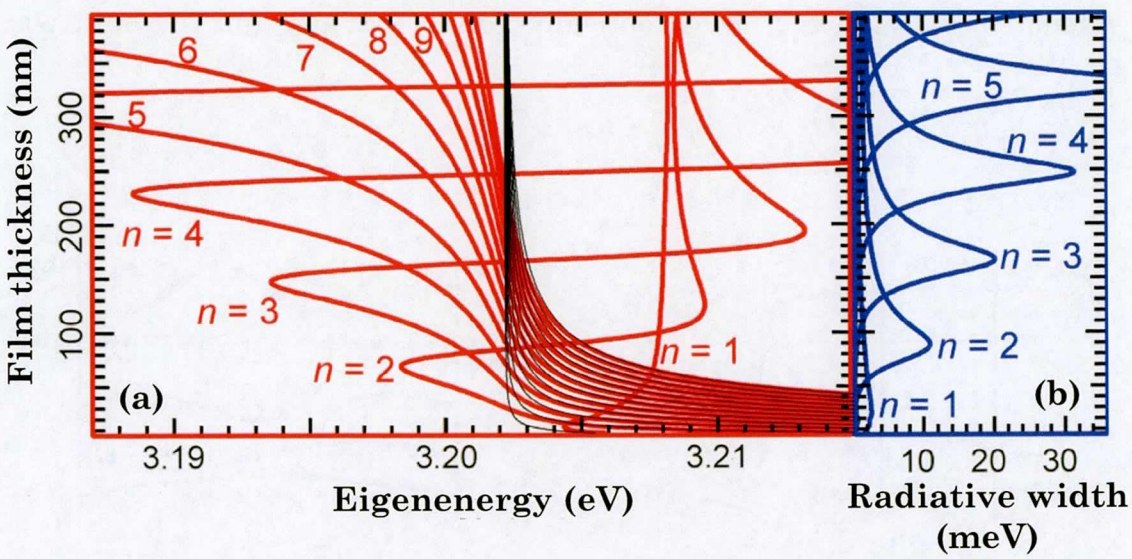

Figure 3.2. *(a) The theoretically calculated eigenenergies of different light-coupled excitonic states whose the quantum numbers are denoted nearby as a function of the CuCl film thickness (red solid lines). That of the uncoupled excitonic states is displayed by black solid lines. (b) The theoretically calculated radiative width (proportional inversely to the radiative lifetime) of different light-coupled excitonic states whose the quantum numbers are also denoted nearby as a function of the film thickness (blue solid lines).*

By considering the spatial interplay between the light and multinode-type excitonic waves, Ishihara *et al.* has calculated theoretically the film thickness dependence of the excitonic state's eigenenergy and radiative width for the case of CuCl as shown in Fig. 3.2. In comparison to the eigenenergy of the uncoupled excitonic presented by black solid lines, the radiative shift of the lowest state is always positive while all other states have negative radiative shift when the thickness is small. For the latter states, the eigenenergies decrease with increase the thickness at the initial stage, but then, they turn to increase and jump to the higher energy side at the certain thickness for respective mode and approach the longitudinal excitonic energy in bulk. The radiative width of each mode reaches maximum at the same time of this jump. Such complicated thickness dependences reflect the change in the phase relation between the excitonic and light waves.

A peculiar nonlinear response contradicting the LWA was reported in GaAs thin film, wherein the size resonant enhancement of the nonlinear signal arises from the nondipole-type excitonic state, which is normally an optically forbidden state [7-8]. By using a method based on nondegenerate two-photon excitation scattering, Syouji *et al.* observed successfully the purely confined excitonic states with not only odd but also even quantum numbers from CuCl thin films [9]. Our group has observed experimentally a

remarkably strong coupling between light and exciton in high quality CuCl thin films with thicknesses of several hundreds of nanometers as an exceptionally short radiative decay time reaching 100 fs [10], which is several orders of magnitude shorter than the typical excitonic nonradiative decay time [11]. The results of theoretical analysis demonstrate that the coupling between the light wave and the extended multinode-type excitonic wave over several wavelengths is formed as long as the wave function of the c.m. motion of exciton is coherently extended over the whole volume of a system [12-13]. In a thin film with very high crystalline quality, the size-dependent increase in the light-matter interaction is no longer limited by the light wavelength and the radiative decay rate is enhanced in a larger system than nanostructures with adequately improved crystalline quality.

3.1.2. Motivations and purposes

In the non-LWA regime, linear optical spectroscopy such as transmittance and reflectance spectroscopy exhibits complicated interference effects between the incident and the scattering fields, and we find that the energies of confined excitons coincide with the peak or dip structures in the spectra if their radiative coupling is not strong [14-15]. However, the quantum levels of lower-numbered states with a strong

radiative coupling are largely shifted from such peak or dip structures, and do not appear in those spectra [16]. Thus, nonlinear methods such as degenerate four-wave mixing (DFWM) and nondegenerate two-photon excitation scattering spectroscopy were used to examine the quantum states of confined excitons [8-10].

In this chapter, we show the experimental evidence that the excitonic states in CuCl thin films, both lower and higher, even and odd quantum numbers, can be observed obviously even by a simple incoherent spectroscopy, namely photoluminescence (PL), provided that the crystalline quality is sufficiently high. By changing the excitation condition from the resonant to band-to-band excitations, the observed mode structures in the PL spectra are confirmed reasonably to originate from the luminescence of the exciton states, not from the resonant scattered one, which is owing to their ultrafast nature in the radiative decay. Based on the qualitative fittings of the PL spectra, the full width at half maximum (FWHM) of the excitonic states can be received and they show the same dependence on the quantum numbers as predicted by the theoretical calculation for all kinds of the excitation conditions. This result indicates that high coherence of matter systems is clearly reflected even in its incoherent photo-processes, which reveals unexploited potential of the PL spectroscopy.

3.2. Experimental details to chapter 3

3.2.1. Degenerate four-wave mixing spectroscopy

3.2.1.1. Four-wave mixing process

The polarization generated by the incident electromagnetic field is initially in phase with the field, i.e. two waves are coherent. The first scattering processes which occur destroy this coherence. The characteristic time in which the fraction of the polarization that is still in phase with the incident field decays to e^{-1} is called the phase relaxation time T_2 or more precisely the decoherence time. The most widely used technique to determine the decoherence time T_2 are based on the four-wave mixing experiment. The concept of three electromagnetic fields interacting to produce a fourth field is central to the description of all four-wave mixing processes. Physically, we may understand these processes by considering the individual interactions of the fields within a dielectric medium. The first input field causes an oscillating polarization in the dielectric medium which re-radiates with some phase shift determined by the damping of the individual dipoles; this is just traditional Rayleigh scattering described by linear optics. The application of a second field will also drive another polarization of the dielectric and the interference of the two waves will cause harmonics in the polarization at the sum and difference frequencies.

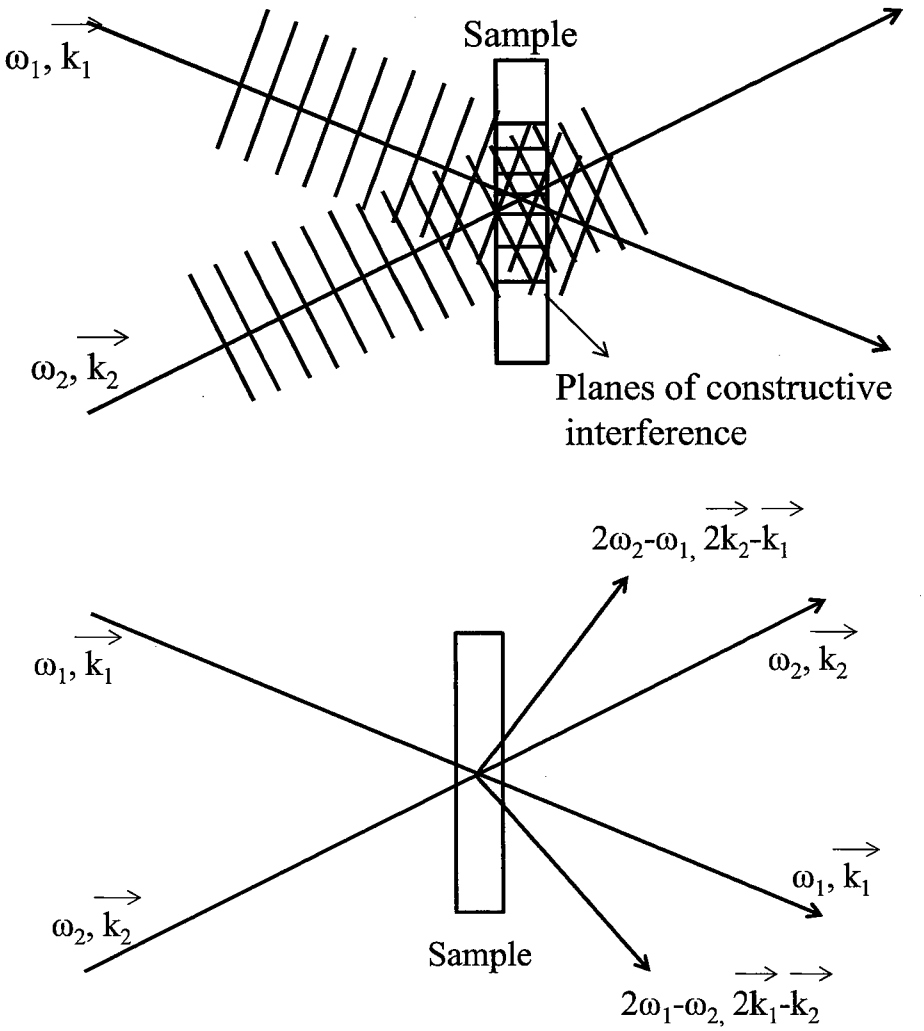

Figure 3.3. *(a) The interference of two incident fields inside the sample. (b) The schematic drawing of non-degenerate four-wave mixing experiment.*

Figure 3.3a shows an example of the wavefronts of the interference between two incident beams inside the sample. Now, application of a third field will also drive the polarization, and this will beat with both the other input fields as well as the sum and difference frequencies. This beating with the sum and difference frequencies is what gives rise to the fourth field in four

wave mixing. By detecting the signal from the fourth field, the decoherence time T_2 could be properly determined. In simple case, one of the two incident fields is considered as the third one and the fourth field then will be generated along the specific direction of $2 * \overrightarrow{k_1} - \overrightarrow{k_2}$(or $2 * \overrightarrow{k_2} - \overrightarrow{k_1}$) and with the frequency of $2\omega_1$-ω_2 (or $2\omega_2$-ω_1). If the frequencies of the incident fields are different, it is called non-degenerate four-wave mixing (NDFWM); otherwise, called degenerate four-wave mixing (DFWM). The schematic of non-degenerate four-wave mixing experiment is displayed in the Fig. 3.3b.

3.2.1.2. Degenerate four-wave mixing experiment setup

Figure 3.4 shows the experimental establishment of the DFWM measurement. DFWM spectra were measured using the second harmonic of a mode-locked Ti:sapphire laser, whose repetition rate and pulse duration were 80 MHz and 110 fs, respectively. Photon energy of the pulse was tuned to approximately the transverse exciton energy. The excitation light was split into two pulses and both of them were focused to the same spot on the sample surface. The delay time between two pulses was controlled by using a delay stage. Polarizations of two pulses were parallel and the delay time was set to zero for our measurement. The DFWM signal obtained along the direction of $2 * \overrightarrow{k_1} - \overrightarrow{k_2}$ or $2 * \overrightarrow{k_2} - \overrightarrow{k_1}$ then was transmitted through an optical

fiber to a 50-cm monochromator equipped with a nitrogen-cooled CCD. The spectral resolution was better than 0.08 meV. CuCl thin films were grown by means of the molecular beam epitaxy (MBE) method as described in Chapter 2. Crystalline quality of the CuCl films was extremely improved by our novel technique of electron beam irradiation at the beginning of MBE growth [17], and experiments using high-quality thin films with very small dephasing constants (Γ) of about 0.2 meV can be feasibly realized. The grown films were mounted in a helium flow cryostat and the temperature was cooled below 10 K.

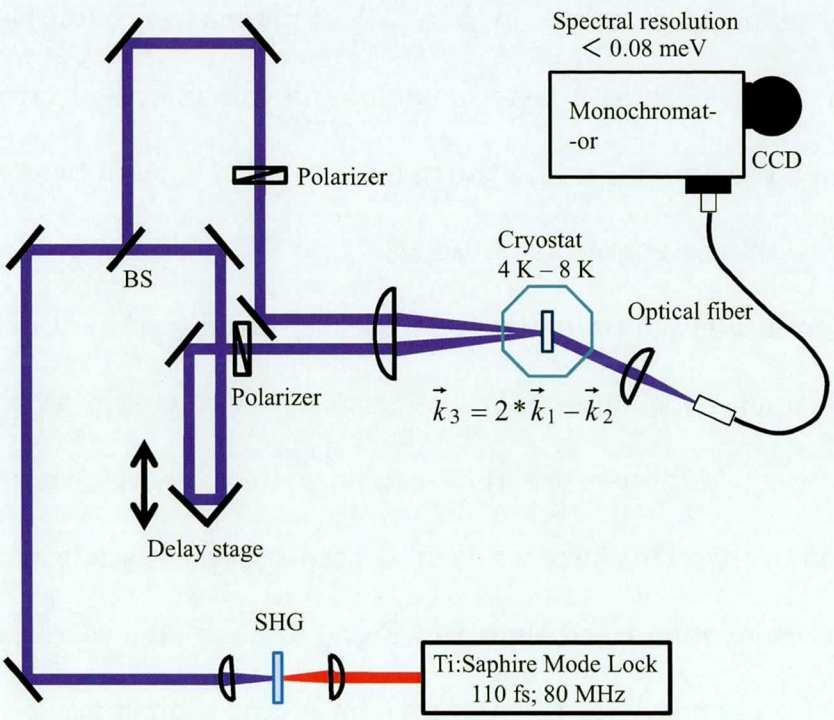

Figure 3.4. *The schematic drawing of the degenerate four-wave mixing experiment for high quality CuCl thin films at low temperature.*

3.2.2. Photoluminescence spectroscopy

3.2.2.1. Photoluminescence process in a semiconductor

Luminescence in solids is the phenomenon in which electronic states of solids are excited by some energy from the external source and the excitation energy is released as light. When the energy comes from light, usually ultraviolet light, the phenomenon is called photoluminescence. CuCl, the material used in my experiment, is a direct semiconductor. Thus, let me discuss generaly about only the photoluminescence process in direct semiconductors. An overview of the photoluminescence process in a direct gap semiconductor is given in Fig. 3.5. Photons are absorbed from an excitation source such as a laser or lamp, and this injects electrons into the conduction band and holes into the valence band. This will be possible if the frequency ν_L of the source is chosen so that $h\nu_L$ is greater than E_g. It is apparent from Fig. 3.5 that the electrons are initially created in states high up in the conduction band. The electrons do not remain in these initial states for very long, because they can lose their energy very rapidly by emitting phonons. This process is indicated by the cascade of transitions within the conduction band shown in Fig. 3.5. Each step corresponds to the emission of a phonon with the correct energy and momentum to satisfy the conservation laws. The electron-phonon coupling in most solids is very

strong and these scattering events take place on time scales as short as 100 fs (i.e. 10^{-13} s). This is much faster than the conventional radiative lifetimes which are in the nanosecond range, and the electrons are therefore able to relax to the bottom of the conduction band long before they have had time to emit photons. The same conditions apply to the relaxation of the holes in the valence band.

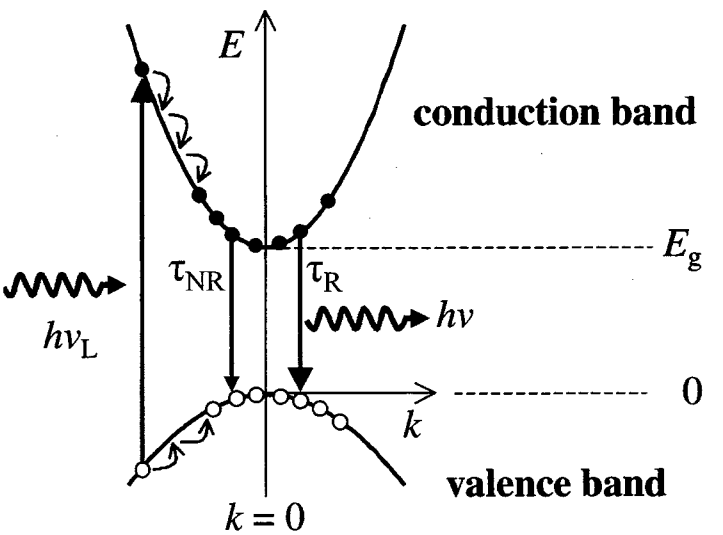

Figure 3.5. *General scheme of photoluminescence in a direct semiconductor.*

After the electrons and holes have relaxed as far as they can by phonon emission, they must wait at the bottom of the bands until they can emit a photon or recombine non-radiatively. The radiative recombination rate is determined by the radiative lifetime τ_R. Radiative emisssion has to compete with the nonradiative recombination which has a time constant of τ_{NR}. The

spectral width of the detected luminesence emission, therefore, contains information of both the radiative and nonradiative processes.

3.2.2.2. Photoluminescence measurement setup

In our experiment, PL spectra were detected in a forward configuration as shown in the Fig. 3.6.

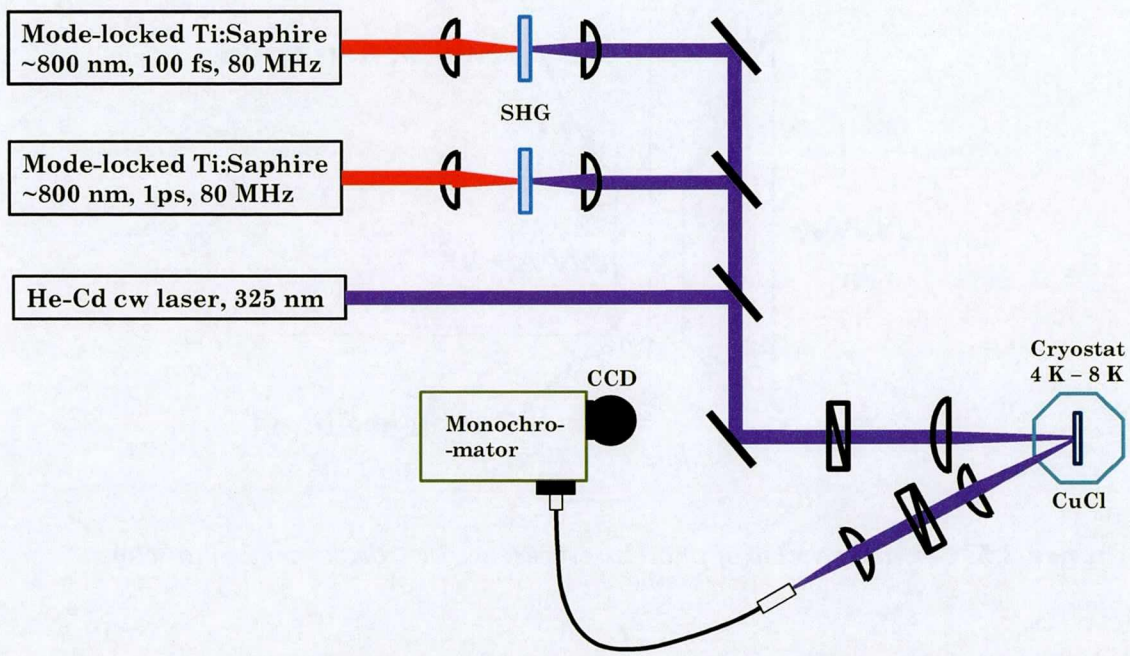

Figure 3.6. *The schematic drawing of photoluminescence measurement for high quality CuCl thin film at low temperature.*

Three other excitation sources were used for different excitation conditions as follows. The second harmonics of two other mode-locked

Ti:sapphire lasers with pulse durations about 100 fs and 1ps were used for the biexciton resonant excitation, while a cw He-Cd laser with an excitation energy of 3.81 eV was utilized for the band-to-band excitation. All the excitation lights were directed to the same position on the sample surface as in the DFWM measurement. To remove efficiently the scattering light of the excitations in the PL spectra, two polarizers with crossing polarizations were used. One was located on the excitation beam path just before the focusing lens, another was placed between two lens, collimating and focusing ones, in the PL detecting system. The PL signal then was collected by the same way used in the DFWM measurement.

3.3. Superradiance of light-coupled excitons in high quality CuCl thin films

3.3.1. Multiple light-coupled modes of confined excitons in degenerate four-wave mixing and photoluminescence spectra

Figure 3.7 shows the DFWM as well as the PL spectra measured under various excitation conditions, including an excitonic resonant fs-pulsed excitation (the excitation energy of 3.202 eV), biexciton resonant fs-pulsed, ps-pulsed excitations (the excitation energy of 3.186 eV) and a band-to-band cw excitation (the excitation energy of 3.81 eV), of the CuCl thin film with a

thickness of 325 nm and a dephasing constant Γ of 0.2 meV derived from fitting of the reflection spectrum at 6 K.

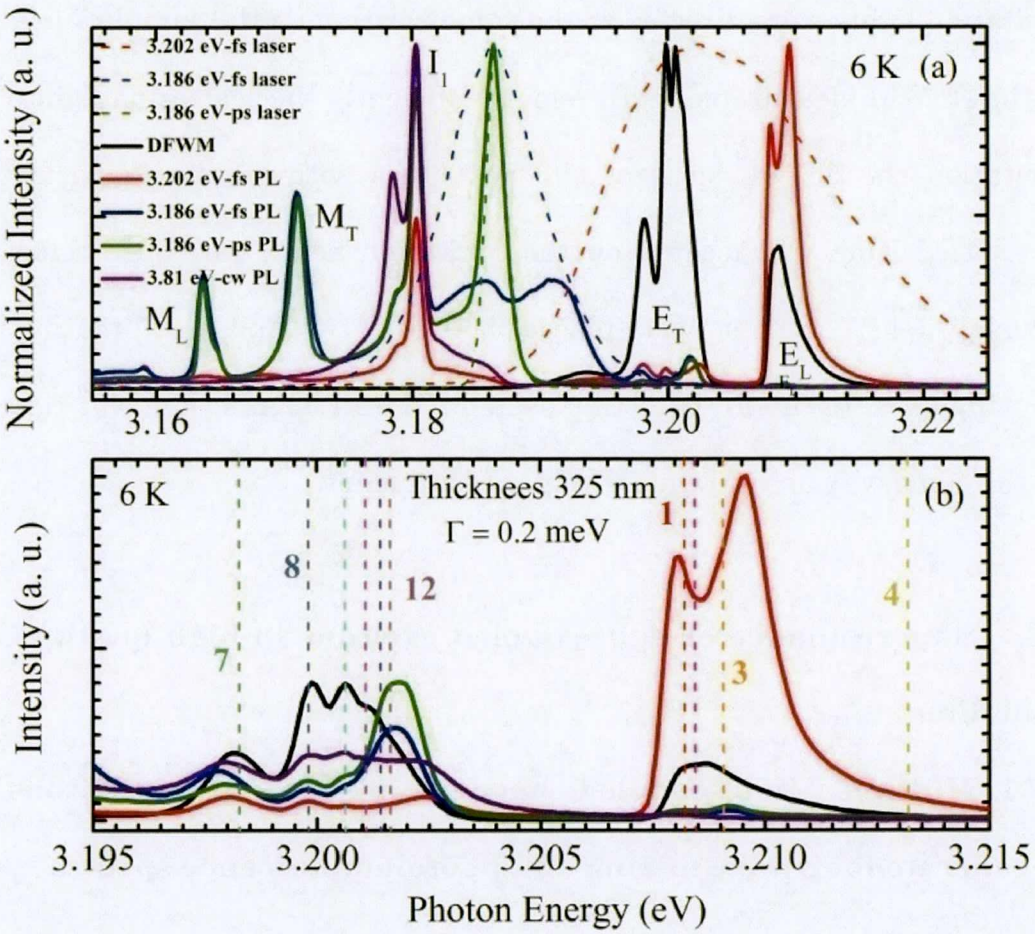

Figure 3.7. *(a) The degenerate four-wave mixing spectrum as well as the photoluminescence spectra measured under various kinds of the excitation conditions (colored solid lines) for a CuCl thin film with a thickness of 325nm and a dephasing constant Γ of 0.2 meV at 6 K. The M_L and M_T bands are the biexciton luminescence resulting from radiative relaxation of excited biexcitons to the longitudinal (E_L) and transverse (E_T) excitonic states, respectively. The I_1 band is*

originated from excitons bound to neutral donors. The dashed lines indicate the different excitation lasers. (b) The degenerate four-wave mixing and photoluminescence spectra expanded in the excitonic energy region. The spectra are multiplied by suitable factors for an easy comparison of the detailed mode structures in the degenerate four-wave mixing and photoluminescence spectra. The theoretical calculations of the energies of excitonic states with different quantum numbers for the film thickness of 325 nm are indicated by the dashed lines.

The measured DFWM spectrum exhibits several peaks, which have never been observed in samples grown by traditional methods. As examined previously for various thicknesses of CuCl thin films [10, 18], the peak photon energies shown in the DFWM spectrum again coincide consistently with the theoretically calculated eigenenergies of the excitonic states indicated by the dashed lines in Fig. 3.7.

It is interesting that the same mode structures as observed in the DFWM spectrum appear obviously in the PL spectra measured under both the resonant and band-to-band excitation conditions. One might think a possibility of the resonant signal scattered from the quantized excitonic levels instead of the excitonic luminescence under the resonant excitations. However, the observation of the same mode structures in the PL spectrum measured under the band-to-band excitation whose photon energy is far away from the excitonic energy levels directly denies the possibility of the

scattered signal. Just after a band-to-band excitation, hot electrons and holes are created individually. The excessive energies of electrons and holes then will be dissipated, for example by phonon interactions, and electrons and holes are finally combined to form excitons at different energy levels. In general case, due to fast nonradiative relaxations, excitons are mostly accumulated at the lowest energy level leading to a dominant luminescent band of this lowest state in PL spectra. However, in our particular situation where the radiative decay rates of high energy levels are comparable or faster than the conventional nonradiative relaxation as discussed later, the luminescent bands from these high energy levels are also possible to appear obviously in the PL spectra. Therefore, the mode structures in the PL spectrum under the band-to-band excitation should be the excitonic luminescent bands.

The integrated intensity of the excitonic emission was presented as a function of the excitation power dependence under the biexciton resonant excitation in Fig. 3.8. The integrated intensity of the excitonic emission shows a nearly quadratic dependence on the excitation power reasonably leading to the relaxation-from-biexciton origin of the observed excitons. Consequently, we conclude that the excitonic luminescence was efficiently detected under various excitation conditions.

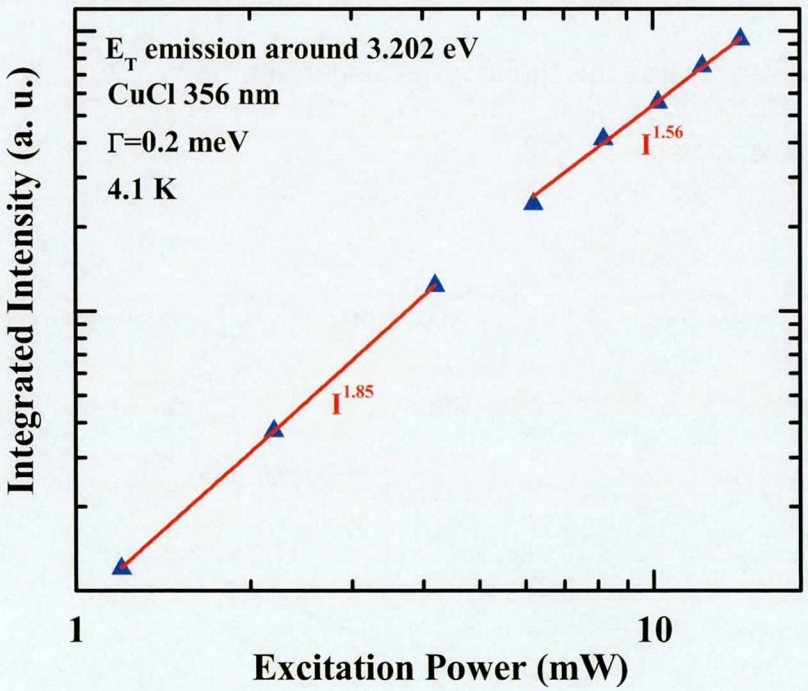

Figure 3.8. *The integrated intensity of excitonic emission around 3.202 eV of a CuCl thin film with a thickness of 356 nm and a damping constant of 0.2 meV as a function of the biexciton resonant excitation power at 4.1 K.*

On the view point of normal polariton dispersion for bulk T. Mita and N. Nagasawa discussed fine structures at excitonic resonance caused by Fabry-Perot fringes in transmission and reflection spectra of a 150-nm CuCl thin film as shown in Fig. 3.9 [14]. They successfully explained the energies of peak and dip structures in the spectra based on the interference of polaritons obeying the dispersion for bulk. However, those energies do not necessarily coincide with exciton modes with radiative correction especially

for the lower-numbered states with strong radiative coupling because they locate far away from the polariton dispersion curve due to the large radiative corrections [9, 12, 13].

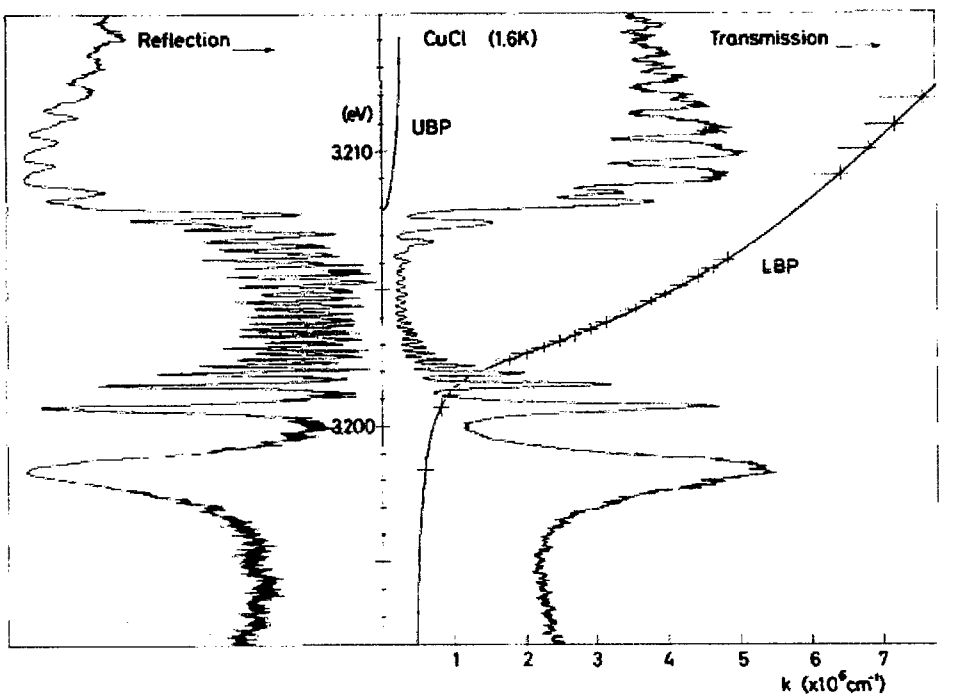

Figure 3.9. *Transmission and reflection spectra in the excitonic region of a CuCl thin film with a film thickness of 150 nm [14].*

In the PL spectra, some peaks corresponding to the excitonic states with even quantum numbers, which are optically forbidden in the LWA regime [3], are observed. In a high quality thin film, strong couplings between the light wave and the multinode-type excitonic waves, not only oddnode-type (odd quantum numbered) but also evennode-type (even

quantum numbered), are formed efficiently and result in fast radiative decay rates of the excitonic states [10], which are much faster than the typical nonradiative dephasing rates [11]. Moreover, differently with other conventional linear spectroscopy such as transmittance and reflectance spectroscopy, the PL spectrum is expected to not contain complicated interferences [14] due to inelastic nature of the response. For the case of excitonic resonant excitation in which there is no differences in photon energy between the excitation light and PL, the incoherent nature of PL would also prevent efficiently just mentioned interferences. As a result, the excitonic luminescence from quantum states with both odd and even quantum numbers, which could only be realized in previous works by nonlinear spectroscopy, can be efficiently obtained by simple PL spectroscopy. In both PL and DFWM spectra, the energy difference between the excitonic state of n=1 and n=2 is so small that the signals contributed from the excitonic state of n=2 could not observe clearly. With the film thickness of 325 nm, the eigenenergy of the exciton state of n=6 is theoretically calculated to be 3.1939 eV locating at the low-intensity tail of the excitation light in the DFWM measurement. Therefore, the signal from the excitonic state of n=6, in fact, still could be observed in the DFWM spectra but with a rather small amplitude. In PL spectra, the luminescent band of the excitonic state of n=6, for this thickness, is close to that of n=5

exciton state (3.19219 eV) whose band width is predicted to be very broad. Thus, it is difficult to see the luminescent band of the excitonic state of n=6 for this film thickness. However, by changing the film thickness, the signals of the excitonic state of n=6 in both DFWM and PL spectra become possible to be observed obviously as shown in Fig. 3.10.

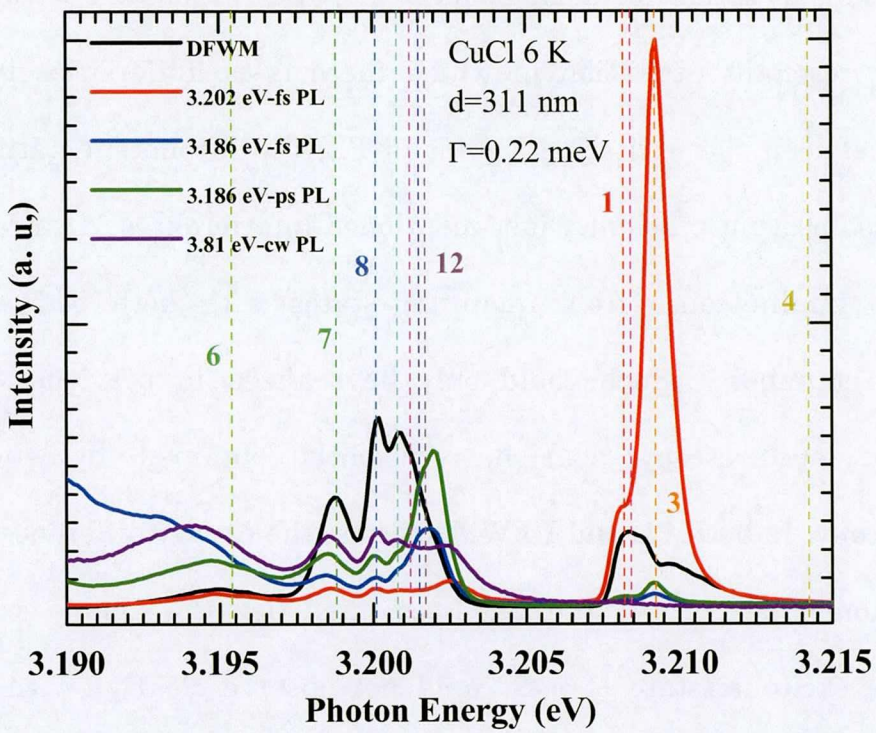

Figure 3.10. *The degenerate four-wave mixing and photoluminescence spectra in the excitonic energy region. The theoretical calculations of the energies of excitonic states with different quantum numbers for the film thickness of 311 nm are indicated by the dashed lines.*

3.3.2. Superradiance of light-coupled excitons in high quality CuCl thin films

To examine characteristics of each excitonic state, it is necessary to identify its contribution in the detected PL spectra. Figure 3.11a and 3.11b show the PL spectra under the biexciton resonant ps-pulsed excitation and the typical fitting curves composed of several Gaussian components around the excitonic transverse and longitudinal energies, respectively.

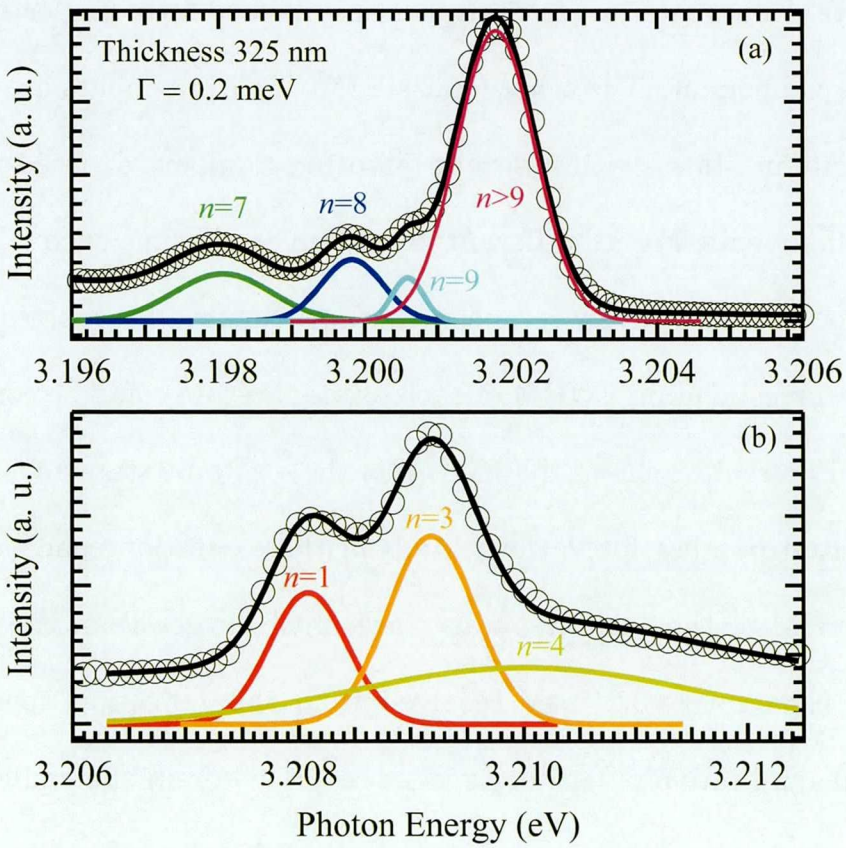

Figure 3.11. *(a) The photoluminescence spectrum in the transverse excitonic energy region under the biexciton resonant ps-pulsed excitation (open circles) and the Gaussian fitting components originating from the excitonic states with the quantum numbers of* n = 7, 8, 9 *and* n > 9 *(colored solid lines). (b) The photoluminescence spectrum in the longitudinal excitonic energy region under the same excitation (open circles) and the Gaussian fitting components originating from the excitonic states with the quantum numbers of* n = 1, 3, 4.

In the fitting process, the overlap of the excited excitonic states with the quantum numbers larger than 9 is assumed to form a spectrally broad Gaussian component. The other Gaussian fitting components are attributed to the excitonic states with different quantum numbers denoted nearby the fitting components. For all different excitation conditions, such a kind of the fitting process qualitatively reconstructs the measured PL spectra.

The corresponding FWHM of each excitonic state could be consequently deduced. Figure 3.12 shows the FWHM of the excitonic state as a function of the quantum number for various kinds of the excitation conditions. These broad FWHM of the excitonic states are much larger than the dephasing damping constant Γ=0.2 meV received from the reflection spectrum and consistent qualitatively with our recent report wherein the radiative decay time, which is inversely proportional to the FWHM of the excitonic state,

reaches the order of 100 fs, much faster than conventional excitonic dephasing processes [10, 18].

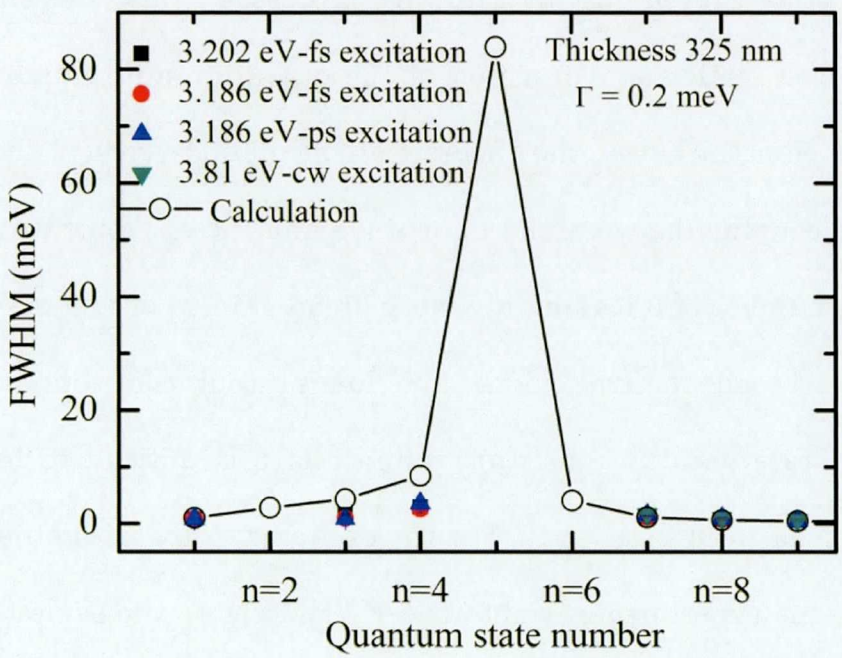

Figure 3.12. *The full width at haft maximum of the excitonic states extracted from the photoluminescence spectra as a function of the respective quantum number under various excitation conditions (solid squares, circles, upward and downward triangles). The theoretically calculated full width at haft maximum of the excitonic states is presented by the open circles.*

No noticeable differences in the FWHM of the same excitonic state are observed with different excitation conditions. In PL spectroscopy, the spectral width of a luminescent band from an excitionic state is determined

primarily by the natural characteristics of the state itself not by the excitation condition which generally causes different rise times in time-resolved spectroscopy. The theoretical calculation of the FWHM of the excitonic state caused only by radiative processes is also presented in Fig. 3.12 by open circles as a function of the quantum state number. For the examined film thickness, the theoretical calculation predicts the strongest harmonic coupling between the light wave and the excitonic wave with the quantum number of 5 leading to a very broad FWHM of ~80 meV [12]. Due to such a broad spectral width, the luminescent contribution from the excitonic state with the quantum number of 5 is difficult to be extracted from the measured PL spectra. For the excitonic states with other quantum numbers, the experimentally obtained FWHM shows the same tendency on the quantum number as the theoretical calculation but with smaller values for small quantum numbers such as n=3, 4. Around the transverse excitonic energy region, the luminescent bands originated from the excitonic states with the quantum state numbers of 7, 8, and 9 are spectrally well separated due to noticeable energy disparities of a few meV leading to an appropriate estimation of the FWHM of each luminescent band. As a result, the FWHM of these excitonic states almost coincide with the theoretical calculation. On the other hand, a considerable overlap between the rather broad luminescent band from the excitonic state with the quantum number n=4

and that from the excitonic state with the quantum number n=3 might lead to an unintentional underestimation of the FWHM of these states in comparison with that predicted by the theoretical calculation.

3.4. Summary

We have shown that if very high quality thin films are prepared successfully, due to a remarkably long coupling length between light and multinode-type excitons, the radiative decay rates of excitonic states even for which locating at high energy levels exceed the nonradiative decay rates because of the ultrafast nature of their radiative processes, which leads to an obvious observation of many excitonic luminescent bands in PL spectra. In this particular situation, the radiative recombination is expected to be still efficient even at high temperatures, therefore, in future, temperature dependent PL spectra might help us to retrieve more useful information for further confirmation of our recent results obtained by means of DFWM spectroscopy [21].

References

[1]. G. D. Scholes, G. Rumbles, Nat. Mat.**5**, 683 (2006) and references therein.

[2]. S. V. Gaponenko, *Optical properties of semiconductor nanocrystals* (Cambridge University Press, 1998).

[3]. Z. K. Tang, A. Yanase, T. Yasui, Y. Segawa and K. Cho, Phys. Rev. Lett. **71**, 1431 (1993).

[4]. T. Takagahara, Phys. Rev. B **39**, 10206 (1989).

[5]. F. C. Spano, and S. Mukamel, Phys. Rev. Lett. **66**, 1197 (1991).

[6]. H. Ishihara, and K. Cho, Phys. Rev. B **53**, 15823 (1996).

[7]. K. Akiyama, N. Tomita, Y. Nomura, and T. Isu, Appl. Phys. Lett. **75**, 475 (1999).

[8]. H. Ishihara, K. Cho, K. Akiyama, N. Tomita, Y. Nomura, and T. Isu, Phys. Rev. Lett. **89**, 017402 (2002).

[9]. A. Syouji, B. P. Zhang, Y. Segawa, J. Kishimoto, H. Ishihara, K. Cho, Phys. Rev. Lett. **92**, 257401 (2004).

[10]. M. Ichimiya, M. Ashida, H. Yasuda, H. Ishihara, and T. Itoh, Phys. Rev. Lett. **103**, 257401 (2009).

[11]. E. Vanagas, J. Kudrna, D. Brinkmann, P. Gilliot, B. Honerlage, Phys. Rev. B **63**, 153201 (2001).

[12]. H. Ishihara, J. Kishimoto, K. Sugihara, J. Lumin. **108**, 343 (2004).

[13]. M. Bamba, and H. Ishihara, Phys. Rev. B **80**, 125319 (2009).

[14]. T. Mita, and N. Nagasawa, Solid State Commun. **44**, 1003 (1982).

[15]. Z. K. Tang, A. Yanase, Y. Segawa, N. Matsuura, and K. Cho, Phys. Rev. B **52**, 2640 (1995).

[16]. See Fig. 3(d) of Ref. 9 and Fig. 3(a) of Ref. 13 and related captions.

[17]. A. Kawamori, K. Edamatsu, T. Itoh, J. Cryst. Growth **237-239**, 1615 (2002).

[18]. M. Ichimiya, M. Ashida, H. Yasuda, H. Ishihara, and T. Itoh, Phys. Stat. Sol. B **243**, 3800 (2006).

[19]. S. Kanemaru, H. Ishiwara and S. Furukawa, J. Appl. Phys. **63**, 1060 (1988).

[20]. R. Bennewitz, D. Smith, and M. Reichling, Phys. Rev. B **59**, 8237 (1999).

[21]. M. Ichimiya, K. Mochizuki, M. Ashida, H. Yasuda, H. Ishihara, and T. Ioth, J. Lumin. **131**,498 (2011).

Chapter 4

Biexciton superfluorescence from an ensemble of CuCl quantum dots

---

As one of essential features for further understandings about biexciton superfluorescence emission from an ensemble of CuCl quantum dots observed recently, the radiative lifetime of biexcitons confined in 3-nm quantum dots was estimated to be about 80 ps under a two-photon resonant excitation by means of time-resolved Kerr gate spectroscopy. Different to the band-to-band excitation, the two-photon resonant excitation is suggested to avoid efficiently the reabsorption process of biexciton luminescence from coexisting excitons leading to a possibility to observe successfully the pure lifetime of confined biexcitons.

4.1. Introduction

In chapter 3, I have touched on excitonic superradiance resulted from the strongly harmonic coupling between the light and multinode-type excitonic waves. In this chapter, I will discuss on some features of another elemental excitation in semiconductors, namely biexciton, relating to superfluorescence (SF) emission, a particular case of superradiance, observed recently [1].

SF occurs due to self-induced synchronization among isolated transition dipole moments through a fluorescence radiation field [2]. SF has been reported mainly for atoms and molecules [3, 4], and those embedded in the solid state [5–8]. However, owing to the quantization of the energy levels of electrons, holes and excitons [9], semiconductor quantum dots (QDs) can be regarded as an isolated quantum system, in addition to being regarded as an ensemble of atoms; hence, an ensemble of semiconductor QDs may possibly exhibit superradiance or SF in the same manner as atoms and molecules do. Furthermore, as a consequence of the radiative time of the exciton being shorter than that for electronic transitions in atoms and molecules, ultrafast radiation or ultrashort pulsed emission can be expected to be typical of cooperative emission from semiconductor QDs.

One of the problems encountered in generating SF in a QD ensemble is the difficulty in achieving complete population inversion for certain pairs of levels through conventional excitation methods. For example, if the exciton state and the ground state are chosen as the two levels for complete population inversion, high excitation intensity is necessary to generate excitons in all the QDs. However, since excitons in QDs are randomly generated following the Poisson distribution, complete population inversion is prevented.

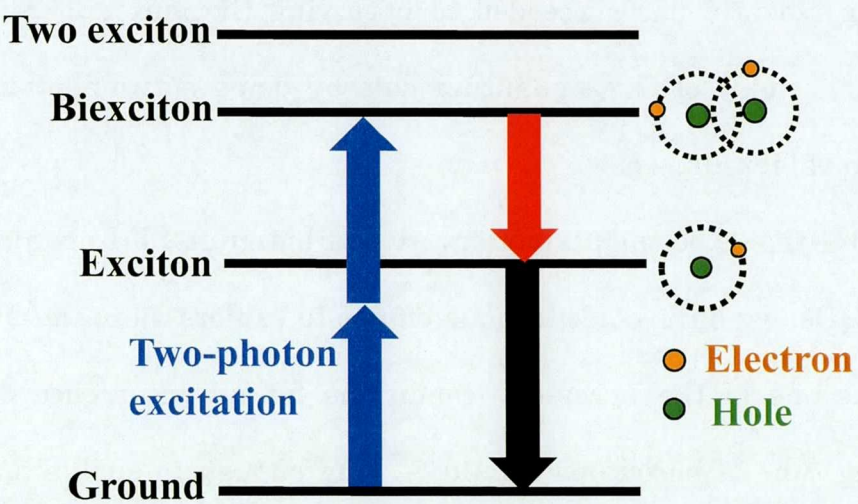

Figure 4.1. *Energy level diagram for the exciton and biexciton states. Blue arrows represent two-photon excitation to the biexciton state. Red and black arrows represent the radiative relaxation of the biexciton and exciton, respectively. The excitation photon energy for resonant two-photon excitation to the biexciton is lower by half the biexciton binding energy compared to the exciton energy.*

In a material with an appropriate biexcitonic binding energy, which is even significantly enhanced in low-dimensional structures due to spatial confinement effect, the resonant two-photon excitation of the biexciton is the most suitable way for achieving complete population inversion [10]. Since the resonant two-photon excitation of the biexciton requires the excitation photon energy to be less than the exciton energy by half the biexciton binding energy, the exciton state at the initial stage is completely unoccupied as shown in Fig. 4.1. Consequently, complete population inversion is realized between the biexciton and exciton states. As a result, our group recently has succeeded in observing the biexciton SF emission from an ensemble of CuCl quantum dots by using a two-photon resonant excitation of biexcitons [11].

After this experimental observation of biexciton SF from an ensemble of CuCl QDs, we have made various efforts to explore more the mechanism of SF. As one of the necessary conditions for an occurrence of SF, the dephasing time of biexcitons should be long enough to enable macroscopic coupling between biexcitons in different QDs. On the view point of how long the dephasing should be for SF emission, a comparison between the dephasing time and the radiative lifetime of biexcitons should be considered. In this chapter, I have estimated the radiative lifetime of biexcitons to be about 80 ps by means of time-resolved Kerr gate spectroscopy under two-

photon resonant excitation of biexcitons. Although, up to date, there is no report on the dephasing time of biexcitons in CuCl QDs, the obtained radiative lifetime is thought to be rather longer than the dephasing time of biexcitons.

4.2. Experimental details to chapter 4

4.2.1. Preparation of CuCl quantum dots embedded in NaCl matrix

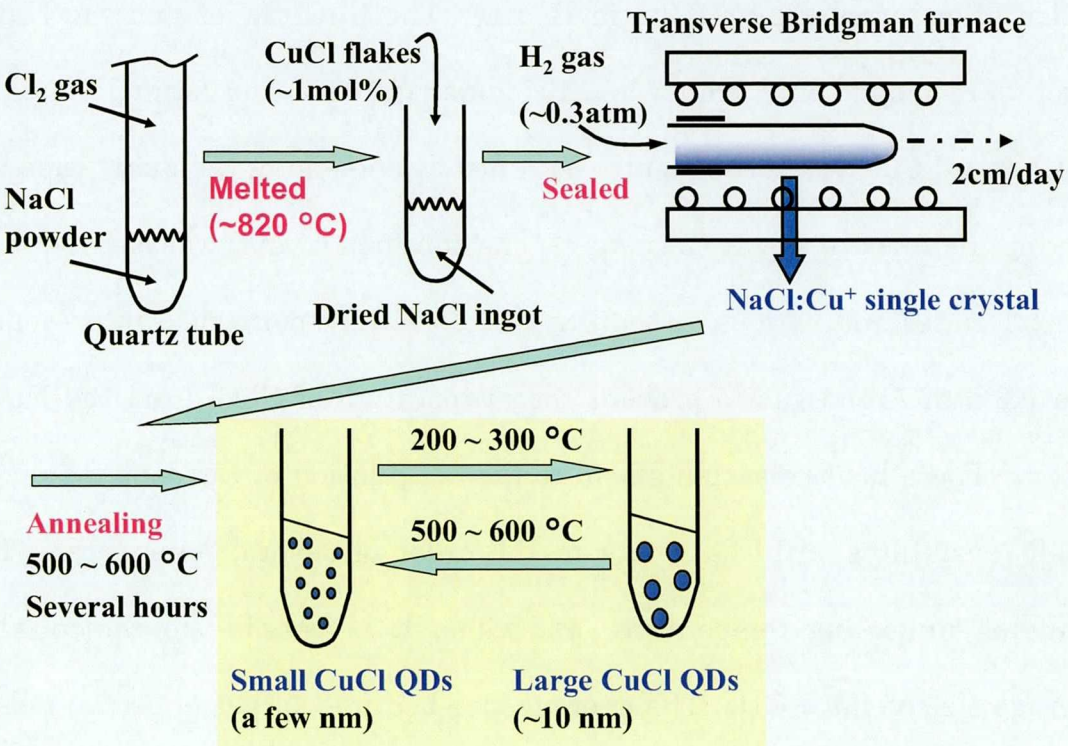

Figure 4.2. *Procedures for the sample preparation of CuCl quantum dots embedded in NaCl matrix by means of transverse Bridgman method followed by subsequent annealing processes.*

CuCl quantum dots embedded in NaCl matrix was fabricated by means of transverse Bridgman method as shown in Fig. 4.2 [12]. The NaCl powder was placed in a quartz tube and heated during a vacuum pumping to remove gaseous impurities. After that, the purified NaCl powder was melted at 820 °C in a sealed quart tube filled by a 0.9-atm Cl_2 gas and the NaCl ingot free from water was obtained. The purified CuCl flakes then were added to the NaCl ingot with a concentration of 1 mol% and the quart tube contained the mixture of the CuCl flakes and the NaCl ingot was sealed after introducing a 0.3-atm H_2 gas. The CuCl flakes and the NaCl ingot were melted in a transverse Bridgman furnace and a single crystal NaCl doped Cu^+ was consequently obtained at one end of the quart tube by moving the furnace slowly (2 cm/day). The obtained crystal was cleaved into several pieces and various annealing processes were performed in presence of a 0.3-atm Argon gas to prevent the evaporation of CuCl from the NaCl matrix. These heat treatments lead to the coagulation of Cu^+ ions to create small crystallites with diameters in the order of several nanometers. By changing annealing temperature and time, it is possible to control the average size of CuCl QDs. The average size becomes larger (~10 nm) when the annealing temperature is in a range from 200 to 300 °C. When temperature reaches to 500-600 °C, the average size becomes smaller (a few nanometers).

4.2.2. Time-resolved Kerr-gate spectroscopy

Figure 4.3a shows a general scheme for time-resolved Kerr gate measurement and the detail effects of the gate light is schematically given in Fig. 4.3b.

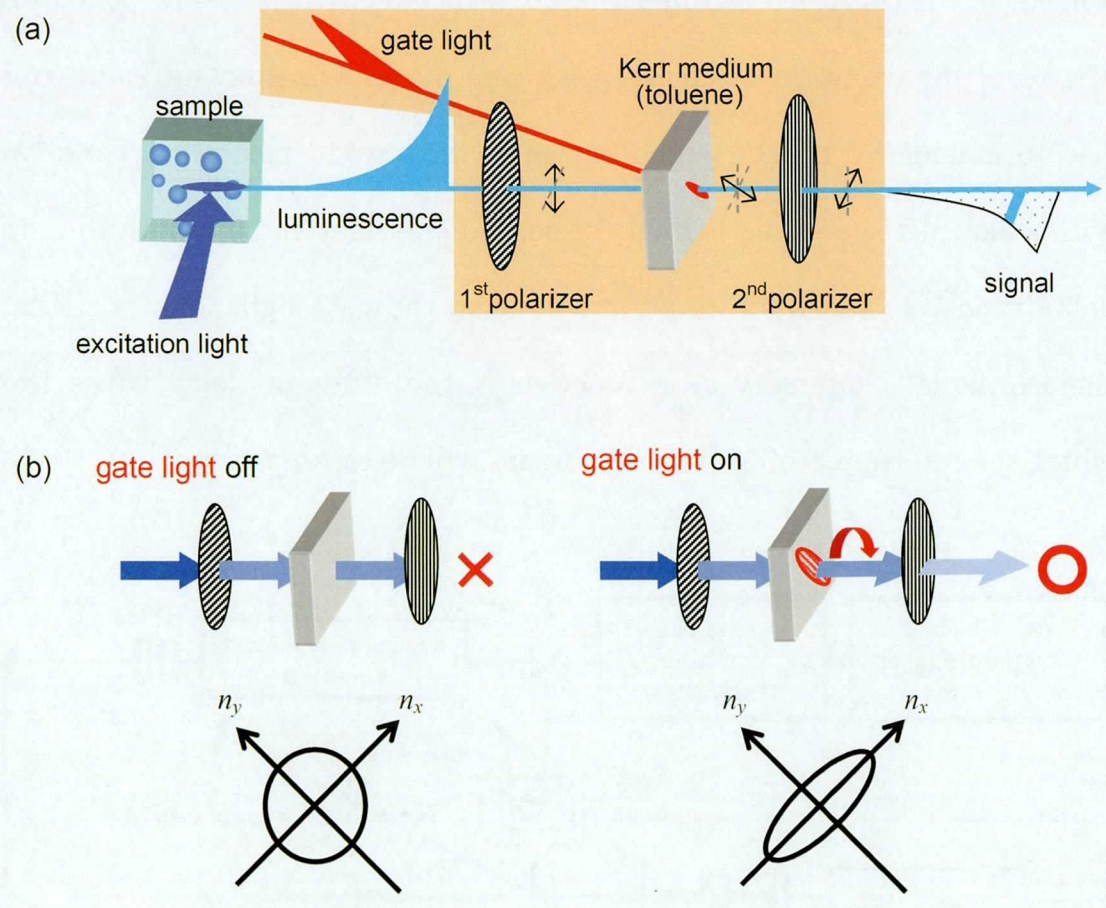

Figure 4.3. *(a) A general schematic diagram of the time-resolved Kerr gate spectroscopy (b) Mechanism of the transmission of luminescence signal through the Kerr cell with and without the gate light.*

The PL signal collected from the sample is non-polarized light, and after transporting two crossing-polarized polarizers of the Kerr nutshell, one can not realize any PL signal at all. But the situation becomes different if a nonlinear optical effect of the Kerr medium, namely the Kerr effect, caused by irradiation of a strong gate light is considered. The gate pulse induces a anisotropy in the Kerr medium placed in between the crossed polarizers. The resulting transient birefringence alters the polarization state and gives rise to leakage of the PL signal through the second polarizer. Therefore, with a slow detector fixed behind the second polarizer and by controlling the delay time between the excitation light and the gate light, one can obtain the PL signal's intensity as a function of the different delay times from which the full time profile of the PL signal will be reconstructed.

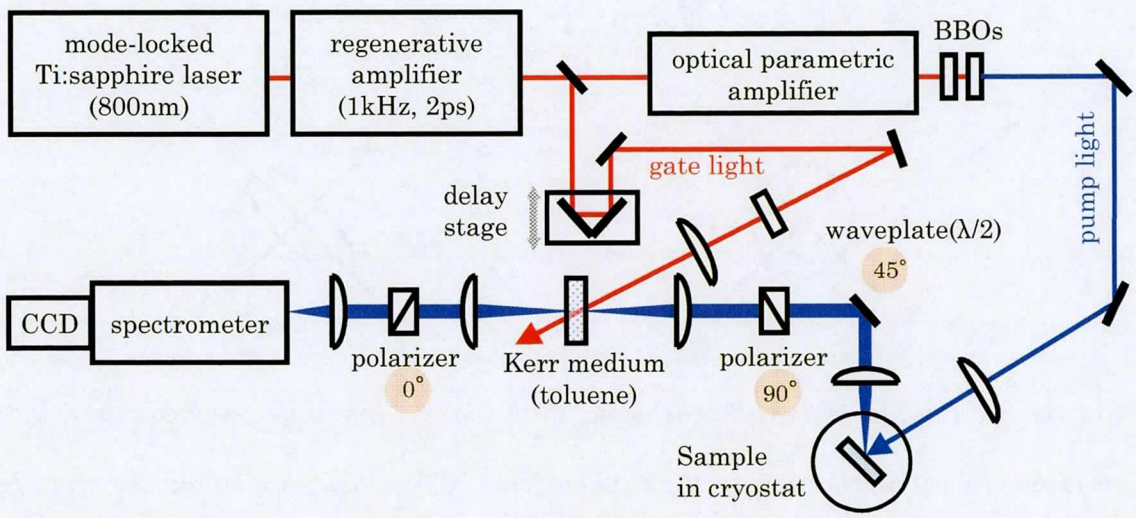

Figure 4.4. *Time-resolved Kerr gate experiment setup.*

Figure 4.4 shows our experimental setup of the time-resolved Kerr-gate spectroscopy. The excitation light is obtained by the fourth harmonic generation of the signal beam from the TOPAS and the excitation wavelengths were tuned to 3.188 eV corresponding to two-photon resonant excitation energy of the CuCl quantum dots with an average radius of 3 nm. The excitation light then was directed and focused on the sample with a spot size of about 110 μm. Photoluminescence signals were collected by a backward scattering geometry, then transferred through a Kerr nutshell including two crossing polarization polarizers and a Kerr medium and finally, focused onto an optical fiber connected to a spectrometer equipped with a liquid nitrogen-cooled CCD array. On the other hand, the regenerative amplified Ti:Sapphire laser (wavelength of ~ 798 nm) is used as the gate light. The strong gate light was defocused on the Kerr medium with a quite lager spot size in comparison with that of the PL to surely make them overlap together. Time-integrated PL spectra were obtained by tuning the angle of the second polarizer so that its polarization is parallel to that of the first polarizer. The CuCl QDs sample was mounted in a He-compressor cryostat and kept at a temperature of 4-5 K. The average size of the CuCl QDs sample used in this study is around ~3 nm defined from one photon absorption spectrum and the thickness of the sample is about ~1.2 mm.

4.3. Biexciton radiative lifetime in CuCl quantum dots

A typical time-integrated PL spectrum of biexciton luminescence from CuCl QDs measured under the resonant two-photon excitation is shown in Fig. 4.5.

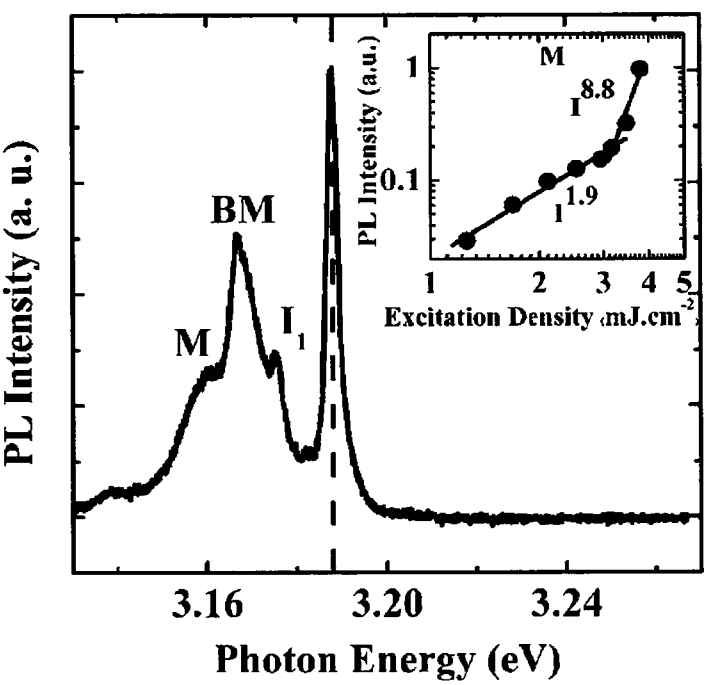

Figure 4.5. *A typical time-integrated photoluminescence spectrum of the biexciton luminescence under the resonant two-photon excitation of 3.188 eV (dash line). The I_1 band is associated with an exciton bound to a neutral donor. The inset shows the excitation density dependence of the photoluminescence intensity of the M band (solid circles) obtained with a backward configuration. The solid lines are the fitting curves with different power factors in the different excitation density regions.*

Two biexciton luminescence bands locating at ~3.16 and ~3.17 eV are denoted as the M and BM bands, respectively. In the previous report, the M band was suggested to relate to the free biexcitons, while the BM to the bound biexcitons since the BM band becomes relatively weak compared to the M band by increasing the temperature [13]. However, the photon energy of M band is not equal to the absorption energy from the exciton to biexciton state [14, 15]. Therefore, we consider that the M band is also a kind of bound state, such as a surface-bound state inherent in the quantum dots. Because the observed characteristics of the BM band are almost the same as those of the M band, discussions of the BM band will be omitted in the following. The excitation density dependence of the integrated intensity of M band is displayed in the inset of Fig. 4.5. The intensity shows a superlinear dependence on the excitation density with the power factors of 1.9 as long as the excitation density smaller than ~2.5 mJ cm^{-2}. In the high excitation density region, meanwhile, the dependent power factor increases dramatically up to a value of 8.8. Such a kind of the behaviour is usually caused by an amplification process. As the number of excited dots is large enough, which should be fulfilled under a high excitation density, and one-round propagation time of the emission light through the excited volume is fairly shorter than the lifetime of the biexcitons in QDs, a luminescence signal from a dot experiences an amplification process during the

propagation through the excited volume. As a result, not only a great enhancement in the PL intensity but also a significant increase in the decay rate is expected. Therefore, an additional examination on the excitation density dependence of the decay time is needed for more reliable confirmation of existence of an amplification process in the high excitation density region.

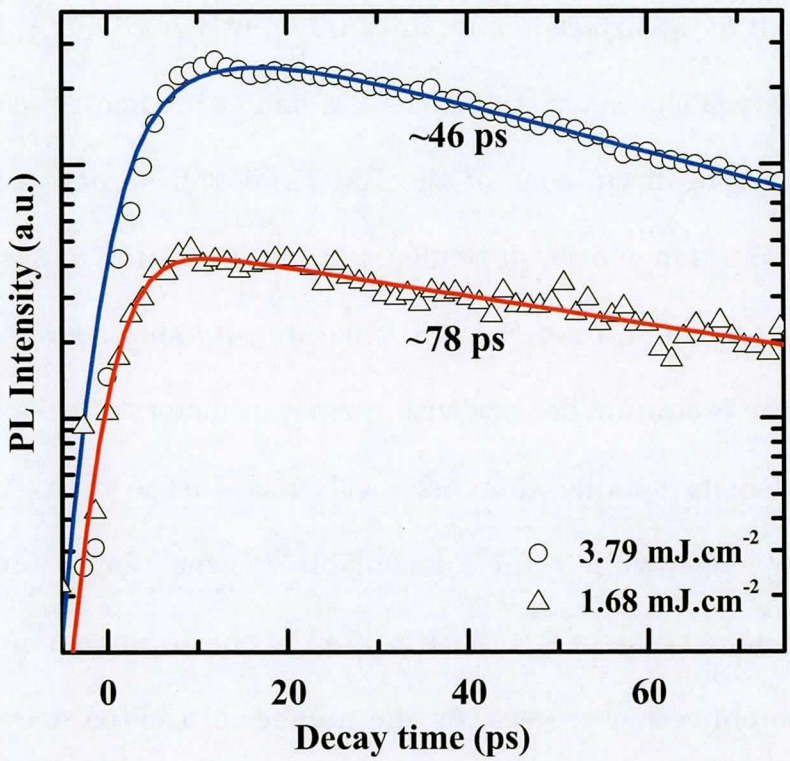

Figure 4.6. *The time profiles of the M band at two different excitation densities (open circles and triangles). The solid lines are the convoluted fitting curves basically consisted of one rise and one decay components with the time profile of the scattered excitation pulse.*

The time profiles of the M band, which basically consist of one rise and one decay component, at two different excitation densities are shown in Fig. 4.6. The rise and decay times of the M band then are extracted by a decovolution analysis and then depicted as a function of the excitation density in Fig. 4.7.

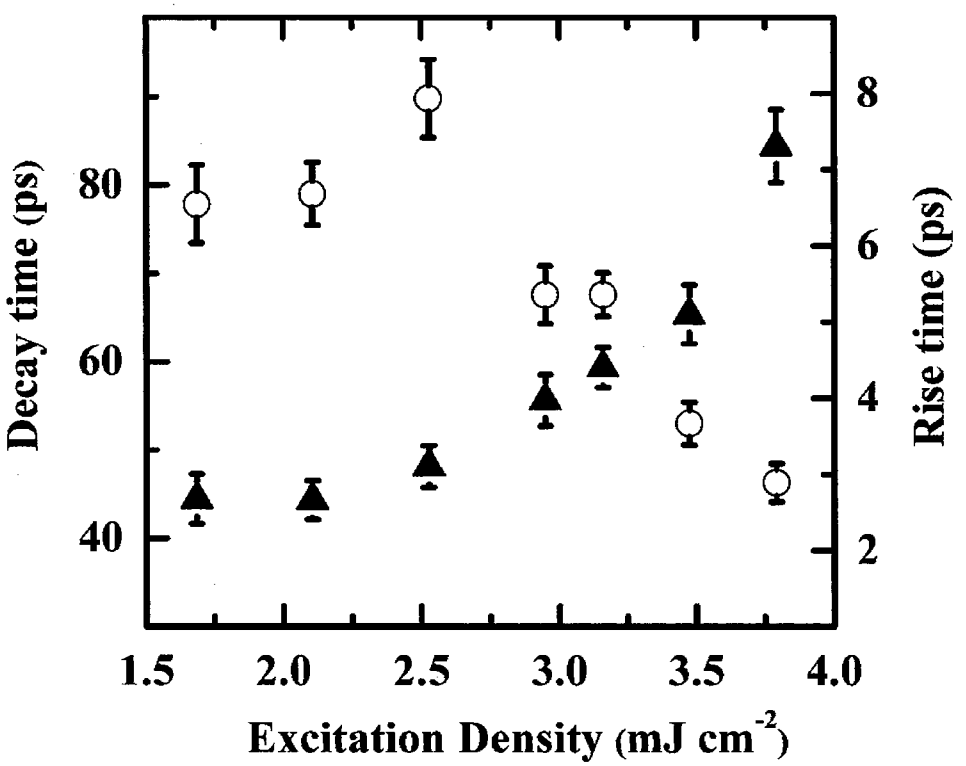

Figure 4.7. *The decay time (open circles) and rise time (solid angles) as a function of the excitation density with the excitation photon energy of 3.188 eV.*

The decay time is almost unchanged, estimated to be about 80 ps, provided that the excitation density smaller than 2.5 mJ cm^{-2}. In the high

excitation density region, the decay time exhibits a decrease with increasing the excitation density. This tendency in the high excitation density region is consistent with expectations subsequently resulted from an amplification process as mentioned. Therefore, basing on the drastic enhancement in the steady PL intensity as well as the decrease of the decay time of the M band, an amplification process is suggested to occur in the high excitation density region. As a result, the unchanged decay time of ~80 ps in the low excitation density region is attributed to spontaneous lifetime of the biexcitons in QDs with an effective radius of ~3 nm.

However, this decay time is not in good agreement with the value of 125 ps previously reported for the lifetime of the free biexcitons under a band-to-band excitation [13]. Figure 4.8 shows a schematic for the reabsorption mechanism which might properly occur under a band-to-band excitation but to be depressed efficiently under a two-photon resonant excitation. With a band-to-band excitation, excitons are generated in all sizes of dots and then collisions between excitons in the same dots lead to creation of biexcitons just after the excitation moment a few ps [16]. Due to a large disparity in the lifetimes of excitons and biexcitons [13, 17], the free biexciton luminescence following a radiative annihilation of a free biexciton in one dot can be reabsorbed resonantly by another same-sized dot inside which one free exciton has already existed, resulting in a regeneration of

another fresh free biexciton. As a result, the decay profile of the free biexciton luminescence will be accumulated and subsequently shows a decay time different from the pure lifetime of biexcitons.

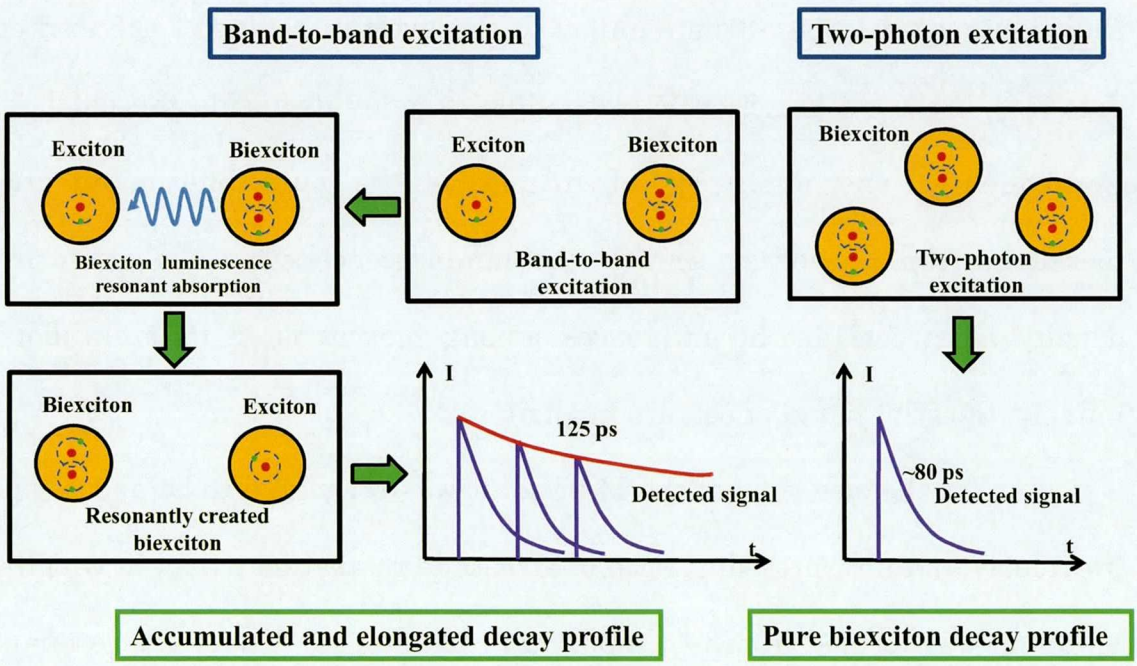

Figure 4.8. *A schematic diagram for the reabsorption mechanism which might properly occur under a band-to-band excitation but to be depressed efficiently under a two-photon resonant excitation.*

On the other hand, with a resonant two-photon excitation of biexcitons by using a picoseconds-pulsed laser possessing a narrow spectral width, the direct generation process of excitons could be neglected completely on account of the large binding energy of biexcions, which is estimated to be about 60 meV for biexcitons in QDs with an average

effective radius of ~3 nm [18-20]. Therefore, the reabsorption process can be removed efficiently under the resonant two-photon excitation. Furthermore, it is different from the bulk crystal that owing to a strong repulsive potential causing by the spatial limitation of the dot and the biexciton Bohr radius supposed to be ~3 nm similar to the average radius of the excited dots [18], a second biexciton is impossible to generate inside the dot [15]. Consequently, one might expect to receive the pure lifetime of free biexcitons from the decay time of the luminescence when the excitation density is as low as the influences among biexcitons in different dots, namely, the stimulated effect, are negligible.

As for the rise time of the M band, it was estimated to be about 3 ps previously and interpreted in term of a cascade relaxation model in which a biexciton was formed from two separated excitons [16]. Under the resonant two-photon excitation, there are two possible sources for the rise time. The first one was proposed that the M band does not relate directly to free biexcitons but to a lower energy level generated by a certain bound state [14, 15]. The other is due to different propagation times of component luminescence signals through the excited volume. The former might contribute constantly to the rise time without any effects from a change in the excitation density. On the other hand, the latter emerges from the fact that the total PL signal was collected from spatially separated dots whose

luminescence are detected at different time moments. The number of excited dots, roughly proportional to the excited volume inside the sample, will be expanded with increasing the excitation density. In the low excitation density region, generation of more excited dots locating at different positions results in the gradually growing rise time of the M band. In the high excitation density region where the amplification process happens, luminescence signals from dots locating near the rear surface of the sample will be amplified efficiently when these component signals transmit through the excited volume to reach the detection system in the backward configuration. Consequently, these signals detected at later time moments become more dominant than those from QDs near the front surface recorded at sooner time moments. Therefore, the rise time of the M band grows up more sharply with changes in the excitation density in high excitation region. The upper limitation of the M band's rise time is mainly determined by the one-round propagation time of the emission light in the sample which is estimated to be about 12 ps.

4.4. Summary

In QDs, it is suggested that the pure lifetime of the biexcions is probably determined under the low excitation density regime in which the

stimulated effect is not supported to occur due to a small number of excited QDs. Due to the spatial volume confinement, it is difficult to create two or more than two biexcitons in one dot. Therefore, only one biexciton will be created in one dot under the two-photon resonant excitation of the biexcitons and with increasing the excitation density, not the number of the biexcitons in one dot but the number of the excited dots will increase. When the excitation density is high enough, that is, a large number of excited quantum dots is created, the biexcitons in different QDs strongly correlates to each other and as a result, the stimulated emission appears. The observed rise time of PL of the biexcitons is attributed to the stimulated effect on the PL signals propagating through the sample to the detecting system with different times.

References

[1]. R. H. Dicke, Phys. Rev. **93**, 99 (1954).

[2]. L. O. Schwan, P. Schwendimann and E. Sigmund, Phys. Rev. A **40,** 7093 (1989).

[3]. M. H. Gibbs, Q. H. F. Vrehen and H. M. J. Hikspoors, Phys. Rev. Lett. **39,** 547 (1977).

[4]. N. Skribanowitz, I. P. Herman, J. C. MacGillivray and M. S. Feld, Phys. Rev. Lett. **30,** 309 (1973).

[5]. R. Florian, L. O. Schwan and D. Schmid, Phys. Rev. A **29,** 2709 (1984).

[6]. M. S. Malcuit, J. J. Maki, D. J. Simkin and R. W. Boyd, Phys. Rev. Lett. **59,** 1189 (1987).

[7]. M. Ashida, H. Arai, O. Morikawa and R. Kato, J. Lumin. **72,** 624 (1997).

[8]. Y. V. Naboikin, S. N. Andrianov, P. V. Zinoview, Y. V. Malyukin, E. N. Rudenko, V. V. Samartsev, N. B. Silaeva and Y. E. Sheibut, Phys. Status Solidi B **135,** 503 (1986).

[9]. S. V. Gaponenko, *Optical Properties of Semiconductor Nanocrystals* (Cambridge University Press, Cambridge, UK 1998).

[10]. K. Miyajima, M. Ashida, T. Itoh, Phys. Status Solidi B **244**, 3297 (2007).

[11]. K. Miyajima, Y. Kagotani, S. Saito, M. Ashida, T. Itoh, J. Phys.: Condens. Matter **21**, 195802 (2009).

[12]. T. Itoh, Y. Iwabuchi, M. Kataoka, Phys. Status Solidi B **145**, 567 (1988).

[13]. S. Yano, T. Goto, T. Itoh, A. Kasuya, Phys. Rev. B **55**, 1667 (1997).

[14]. M. Ikezawa, Y. Matsumoto, Japan. J. Appl. Phys. **36**, 4191 (1997).

[15]. K. Miyajima, M. Ashida, T. Itoh, Phys. Status Solidi B **244**, 3297 (2007).

[16]. S. Yano, A. Yamamoto, T. Goto, A. Kasuya, Phys. Rev. B **57**, 7203 (1998).

[17]. T Itoh, M Furumiya, T Ikehara and C Gourdon, Solid State Commun. **73**, 271 (1990).

[18]. T. Itoh, Nolinear Opt. **1**, 61 (1991).

[19]. K. I. Kang, A. D. Kepner, S. V. Gaponenko, S. W. Koch, Y. Z. Hu, N. Peyghambarian, Phys. Rev. B **48**, 15449 (1993).

[20]. Y. Masumoto, S. Okamoto, S. Katayanagi, Phys. Rev. B **50**, 18658 (1994).

Chapter 5

Summary

This thesis focuses on superradiance nature, ultrafast response times, of excitons and biexcitons in confined semiconductor nanostructures. The excitonic superradiance could be obtained as a result of coherent light-exciton coupling when the quality of semiconductor nanostructures is sufficiently high so that the excitonic wavefunctions extend coherently over the whole volume of the nanostructures. On the other hand, biexcitonic superradiance or more exactly, biexciton superfluorescence is obtained by a macroscopic coherent coupling between biexcitons confined in a large number of nanoparticles.

In chapter 2 and chapter 3, the excitonic states with broad luminescent bands, or ultrafast radiative rate as predicted by theoretical calculation, were possible to be observed just by incoherent photoluminescence due to a great improvement of the CuCl thin film's quality realized by means of electron-beam-assisted molecular beam epitaxy. These ultrafast radiative rates of light-coupled excitons are much faster than the conventional excitonic dephasing rate, such as phonon-assisted relaxation rate, and the

radiative recombination is expected to be still efficient even at high temperature leading to a possibility to use CuCl as a promising material for practical applications. These results also provide a clear example showing that the straightforward control of the size and quality of conventional structured materials can considerably enhance the degree of freedom enabling the development of novel material functions. Hence, further studies on similar effects involving other types of materials with a large excitonic effect, such as ZnO, GaN and organic materials, are required in order to explore the hidden potential of photonic functions.

In chapter 4, two-photon resonant excitation of biexciton was utilized for the purpose of size-selected excitation as well as to extinguish the reabsorption process which obscures the real biexciton lifetime under a band-to-band excitation. Although the dephasing time of biexcitons confined in nanoparticles has not yet been obtained so far, the obtained biexciton radiative lifetime of about 80 ps is suggested to be rather larger the dephasing time of biexcitons. As the radiative lifetime of biexciton is quite longer than the dephasing time, a macroscopic coherent coupling between biexcitons acting as dipole moments in different nanoparticles is possible to obtain leading to an observation of superfluorescence emission. For further understandings about superfluorescence, the four-wave mixing experiment should be done to obtain directly the dephasing time of biexcitons in

nanoparticle although the four-wave mixing signal is predicted to be very small for nanoparticle samples.

Appendix 1

Publications and presentations

Publications:

1. **L. Q. Phuong**, M. Ichimiya, H. Ishihara and M. Ashida, "Multiple light-coupling modes of confined excitons observable in photoluminescence spectra of high-quality CuCl thin films", Physical Review B **86**, 235449 (2012).
2. **L. Q. Phuong**, K. Miyajima, K. Maeno, T. Itoh and M. Ashida, "Transitions from spontaneous emission to stimulated emission and superfluorescence of biexcitons confined in CuCl quantum dots", Journal of Luminescence **133**, 77 (2013).
3. M. Ichimiya, **L. Q. Phuong**, M. Ashida, and T. Itoh, "Growth of high-quality CuCl thin films by a technique involving electron-beam irradiation", Journal of Crystal Growth in press (2013).

Presentations:

1. **L. Q. Phuong**, K. Miyajima, K. Maeno, T. Itoh and M. Ashida, "Transitions from spontaneous emission to stimulated emission and superfluorescence of biexciton confined in CuCl quantum dots", 16th International Conference on Luminescence (ICL'11), Ann Arbor, Michigan, USA, 2011.
2. **L. Q. Phuong**, K. Miyajima, K. Maeno, T. Itoh and M. Ashida, "Possible transitions of biexciton luminescence confined in quantum dots", 24th International Conference on Amorphous and Nanocrystallines Semiconductor (ICANS 24), Nara, Japan, 2011.
3. **L. Q. Phuong**, M. Ichimiya, H. Ishihara and M. Ashida, "Coherent exciton-light couplings in high-quality CuCl thin films", 8th Handai Nanoscience and Nanotechnology International Symposium, Osaka, Japan, 2012.